Supporting information:

A systematic study of the influence of ligand field on the magnetic dynamics of Co(II)-diimine compounds

Indrani Bhowmick[a], Brian S. Newell[a,b] and Matthew P. Shores[a]*

[a] *Department of Chemistry, Colorado State University, Fort Collins, CO 80523-1872, USA, E-mail: matthew.shores@colostate.edu*

[b] *Analytical Resources Core, Center for Materials and Molecular Analysis, Colorado State University, Fort Collins, Colorado 80523, United States*

Table of Contents

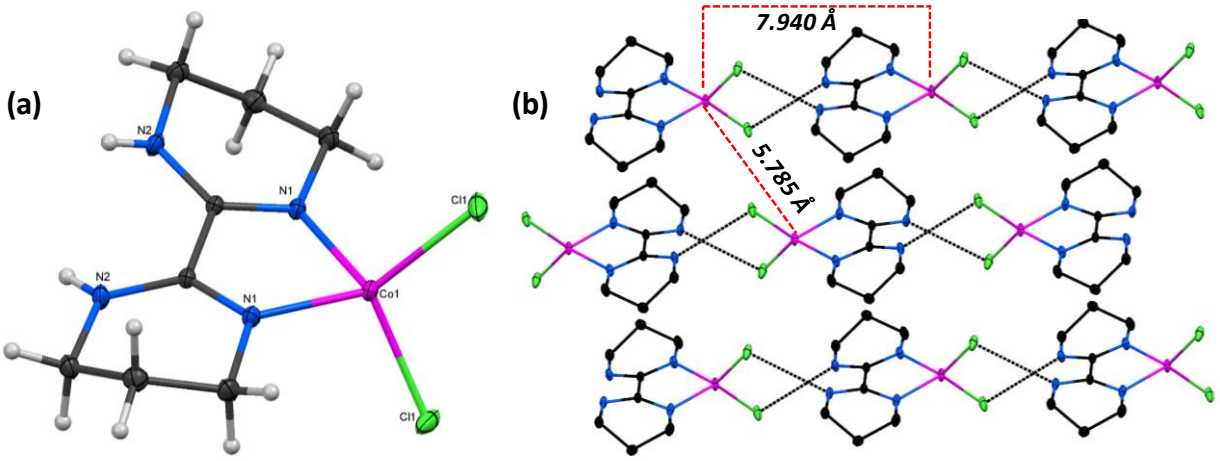

Figure S1: The crystal structure of compound **1a**. (a) ORTEP view with thermal ellipsoids at 50 % probability level. The magenta, green, blue and grey sphere represent the Co, Cl, N, and C atoms. Hydrogen atoms are omitted for clarity. (b) The hydrogen bonded pseudo-one-dimensional chain-like geometry along the b axis and the Co---Co short range distances.

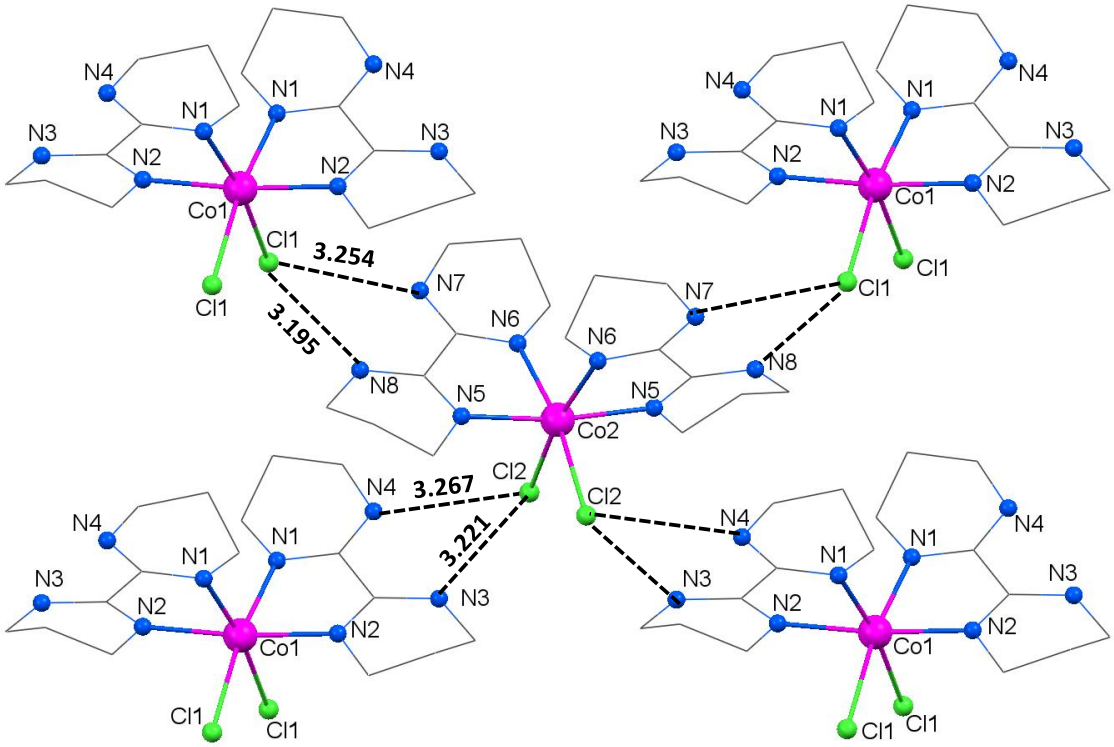

Figure S2: Hydrogen bonding interactions (in Å) in compound **1**.

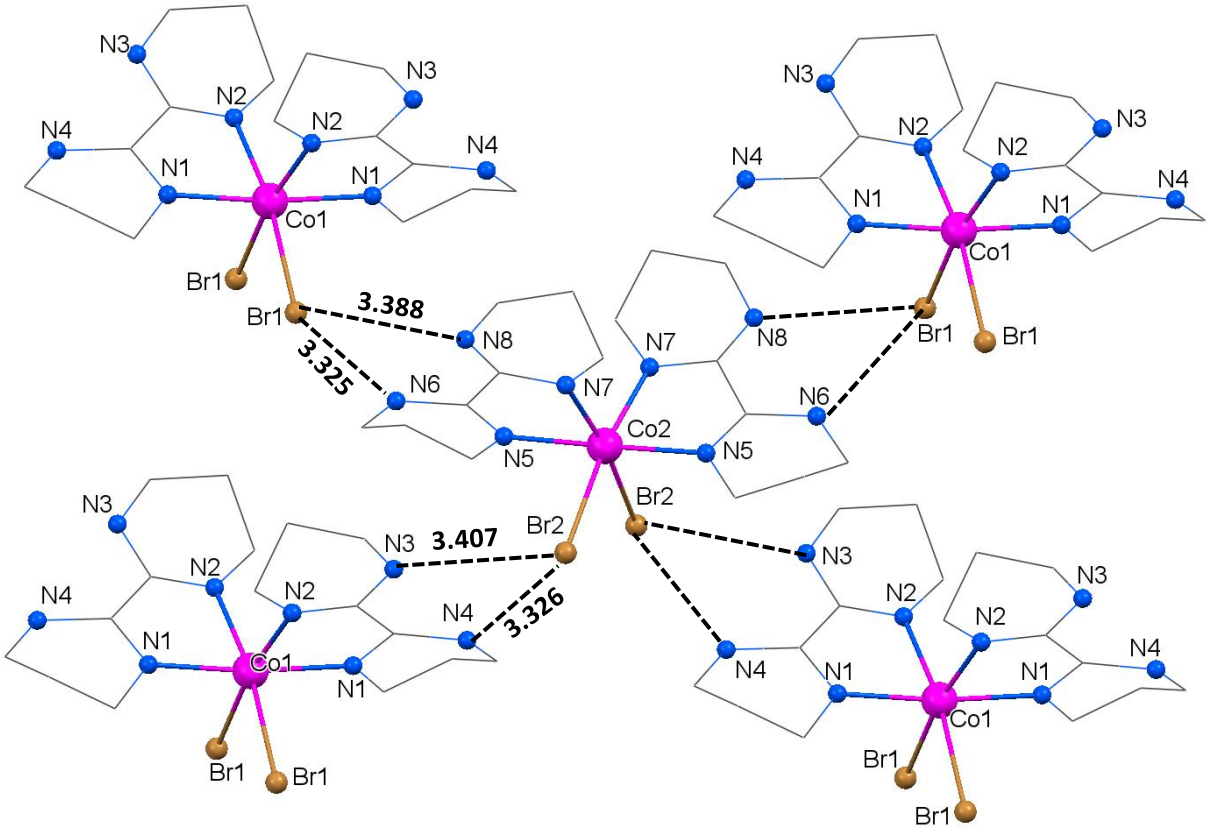

Figure S3: Hydrogen bonding interactions (in Å) in compound **2**.

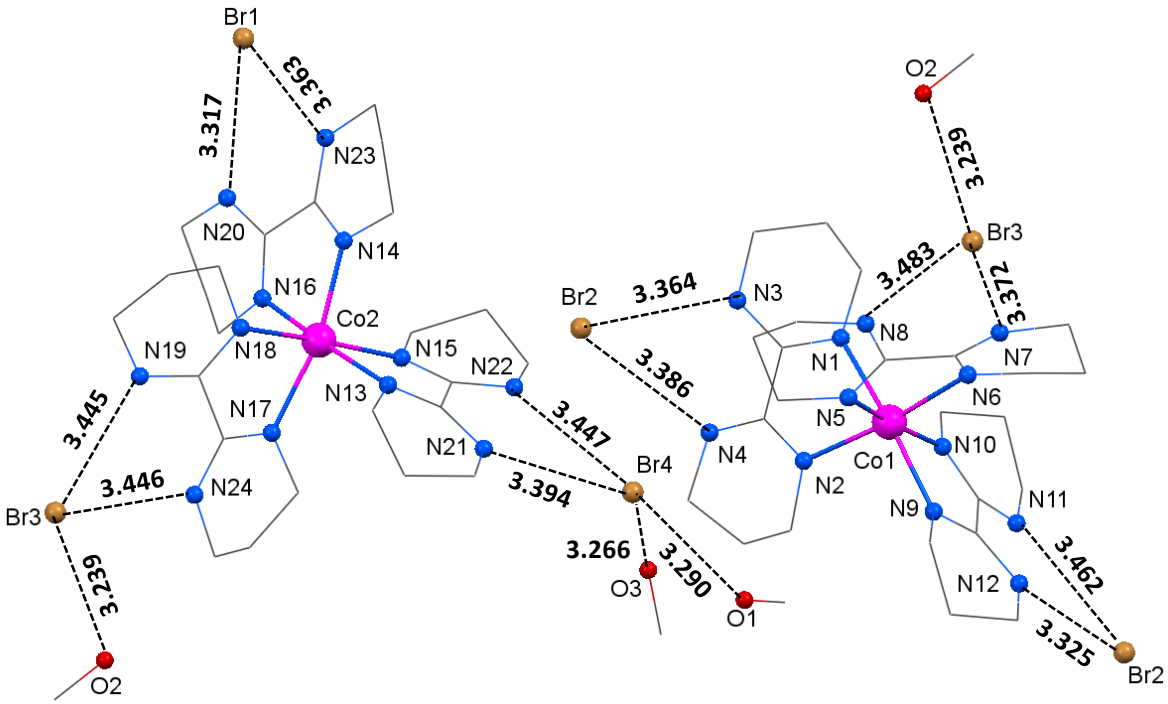

Figure S4: Hydrogen bonding interactions (in Å) in compound **3**.

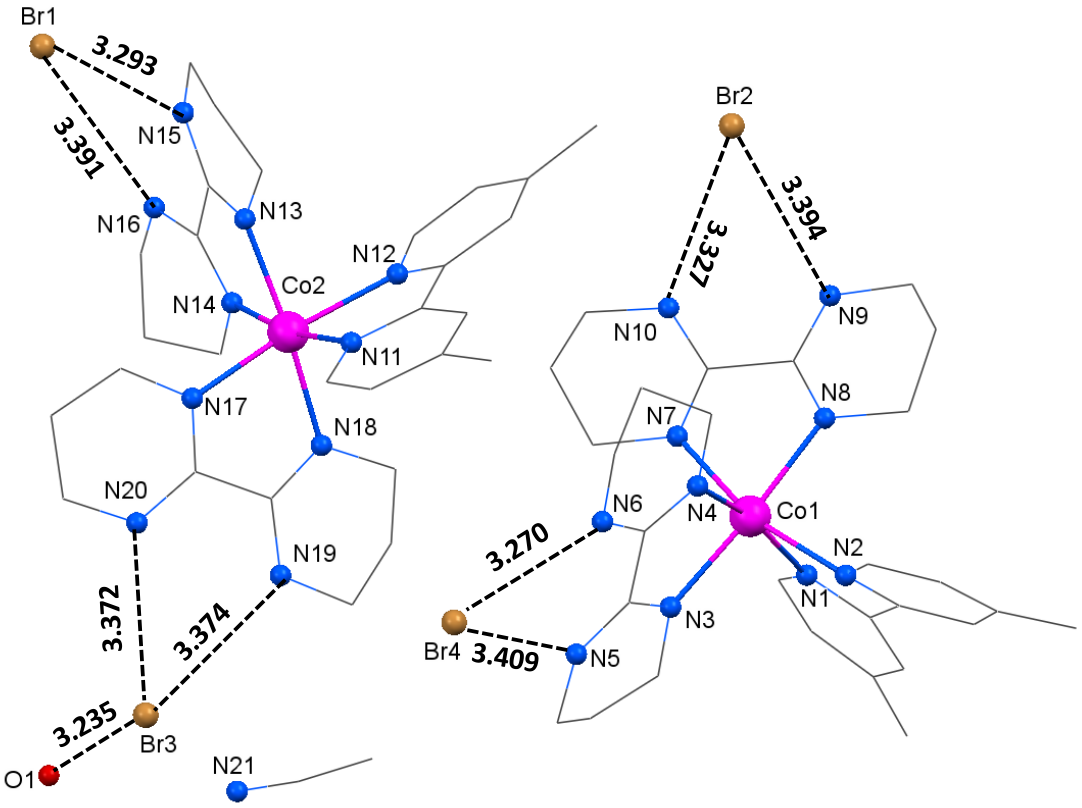

Figure S5: Hydrogen bonding interactions (in Å) in compound **4**.

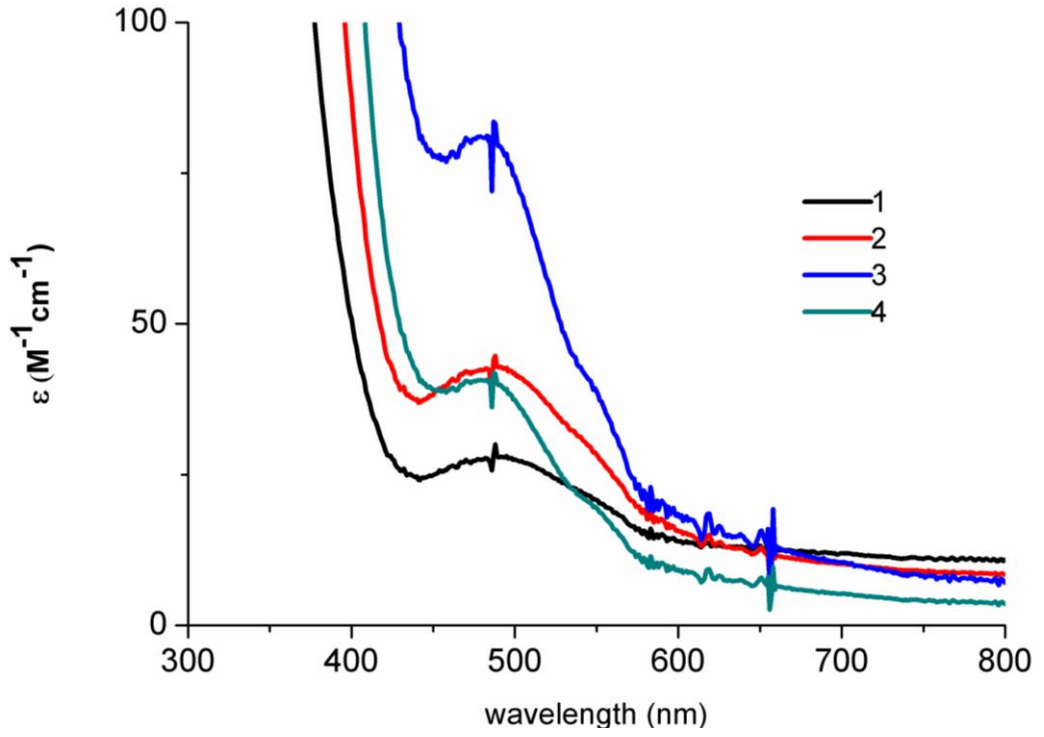

Figure S6: UV-Visible spectra of compounds **1-4** in methanol.

The UV-Vis data collected at MeOH (Fig. S6) showed visible spectrum maxima at 512 nm (19531 cm^{-1}), 494 nm (20243 cm^{-1}), 491 nm (20367 cm^{-1}) and 488 nm (20492 cm^{-1})

respectively for compounds **1-4.** The ground state of the Co(II) O_h high spin compounds are $^4T_1$ and the optical transitions between $^4T_1$ to $^4T_2$ are usually much lower energy (near infrared range). Therefore, the above transitions probably correspond to metal -ligand charge transfers (MLCTs). From the energy distribution shown in Fig. 7 the transitions from the $^4T_1$ to $^4T_2$ states are calculated as 8850 cm^{-1} (1129 nm), 8400 cm^{-1} (1190 nm), 10100 cm^{-1} (990 nm) and 11200 cm^{-1} (891 nm) correspondingly from compounds **1** to **4**. We see increasing magnitude of the metal-based transition energy is noticeable as the π-acceptor property increases in compound **4**. Note that these values are based on approximations and we have not seen these transitions in the UV-Vis spectra collected below 800 nm (Fig. S6). In practice these transitions are more likely to be found at lower energies due to mixing of the ground state and the other low-lying excited states, but the trend should persist in this system.

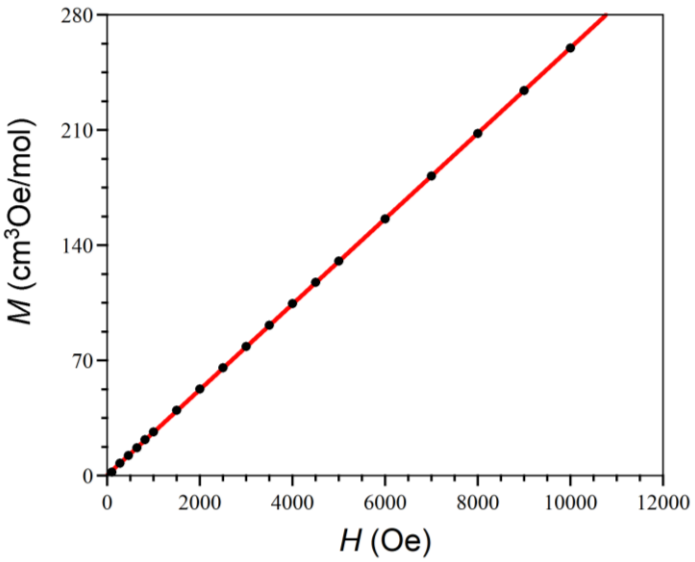

Figure S7: *M* vs *H* plot of compound **1a** at 100 K, the solid black circles are experimental data, and the solid red line is fit of the experimental data. The linear fit (R^2 = 0.999) indicates the absence of the ferromagnetic impurities.

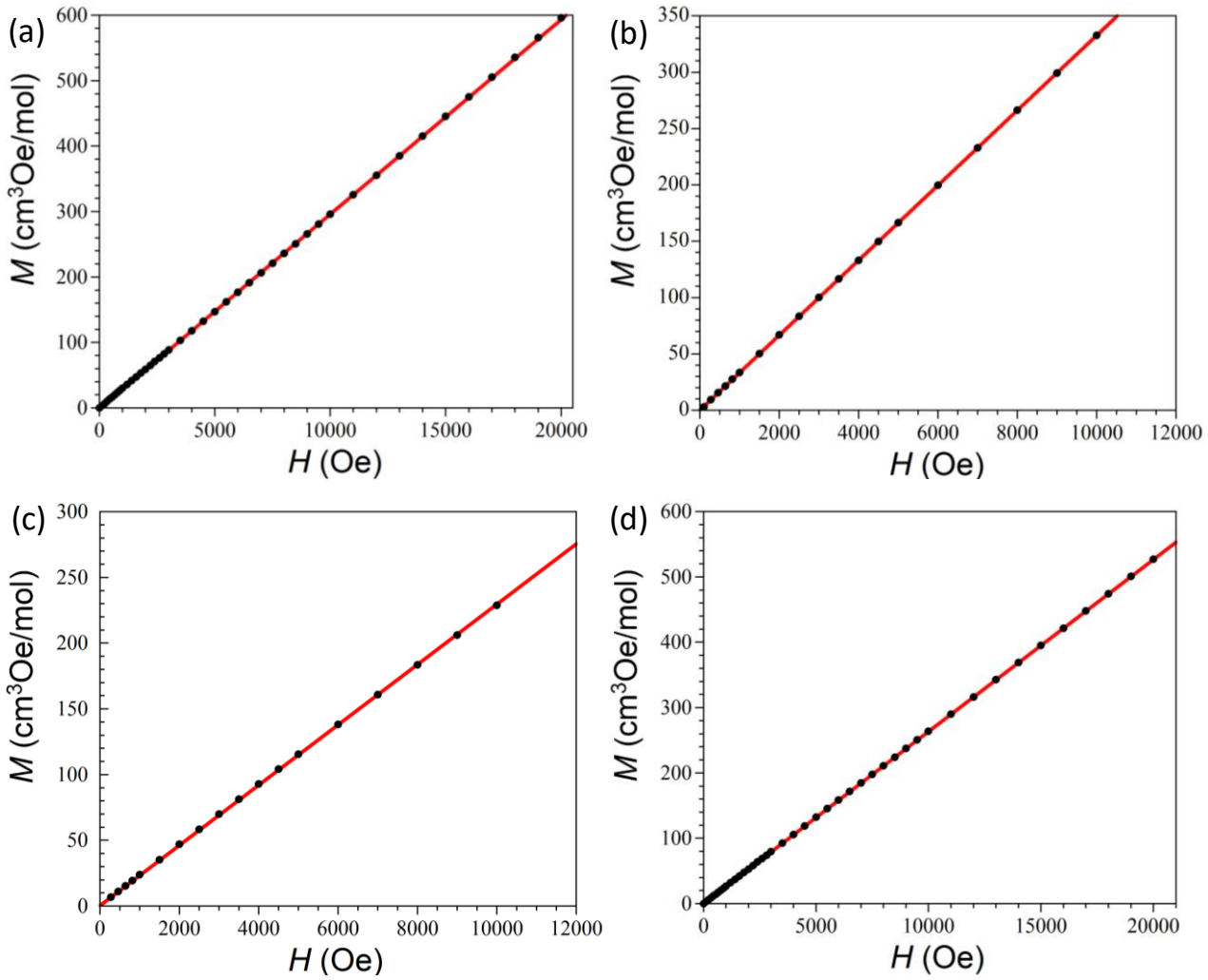

Figure S8: *M* vs *H* plots of compounds **1-4** at 100 K ((a) for **1**, (b) for **2**, (c) for **3** and (d) for **4**), the solid black circles are experimental data, and the solid red line is fit of the experimental data. The linear fits (R^2 values for compounds **1-4** are 0.999, 1, 0.999 and 1, respectively) indicate the absence of the ferromagnetic impurities in all four compounds.

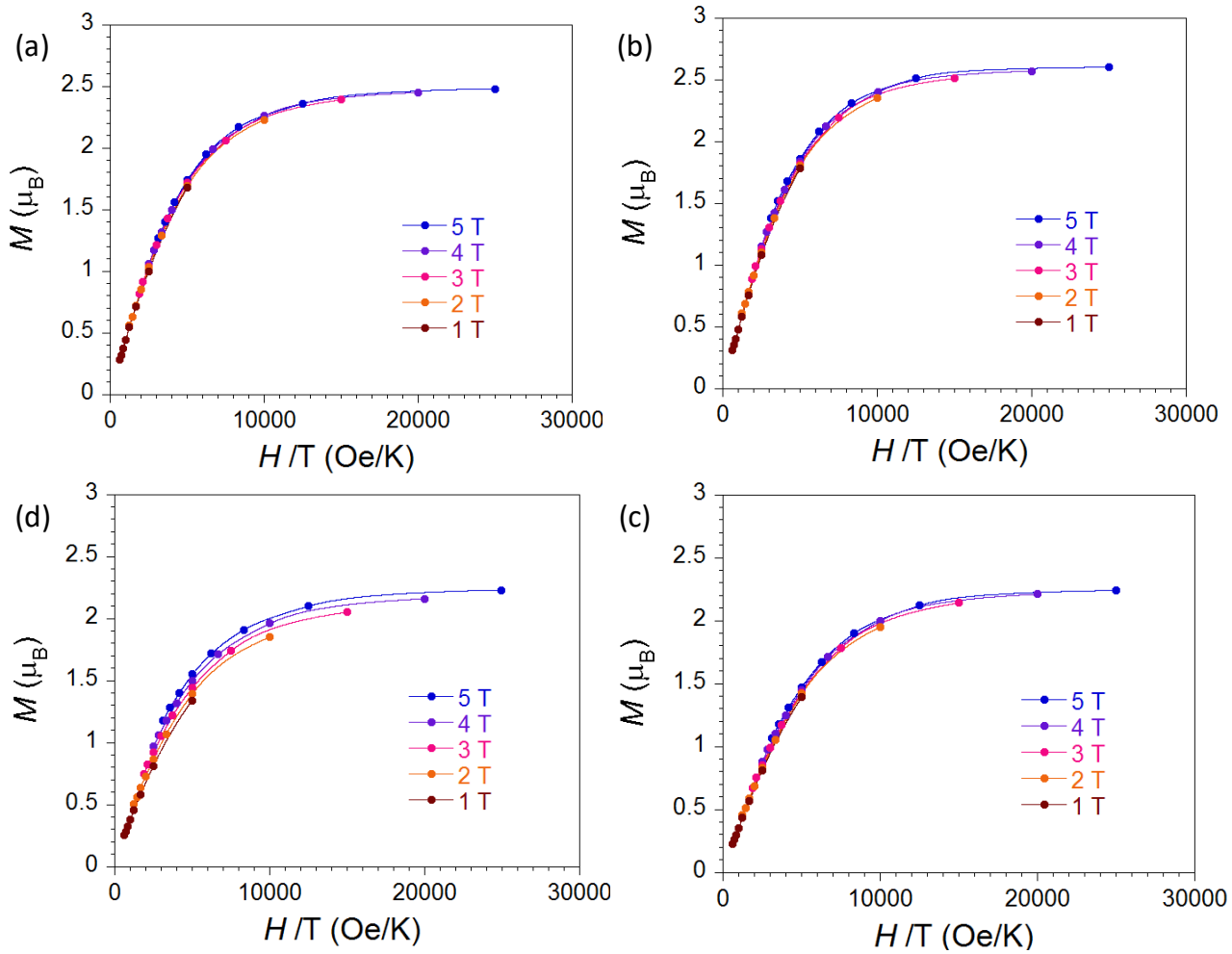

Figure S9: *M* vs *H*/*T* curves for **1** (a), **2** (b), **3** (c), **4** (d). Lines are of best fit determined by fitting in ANISOFIT2.0. The D, E and g values are listed in the table S1 (the black coloured data).

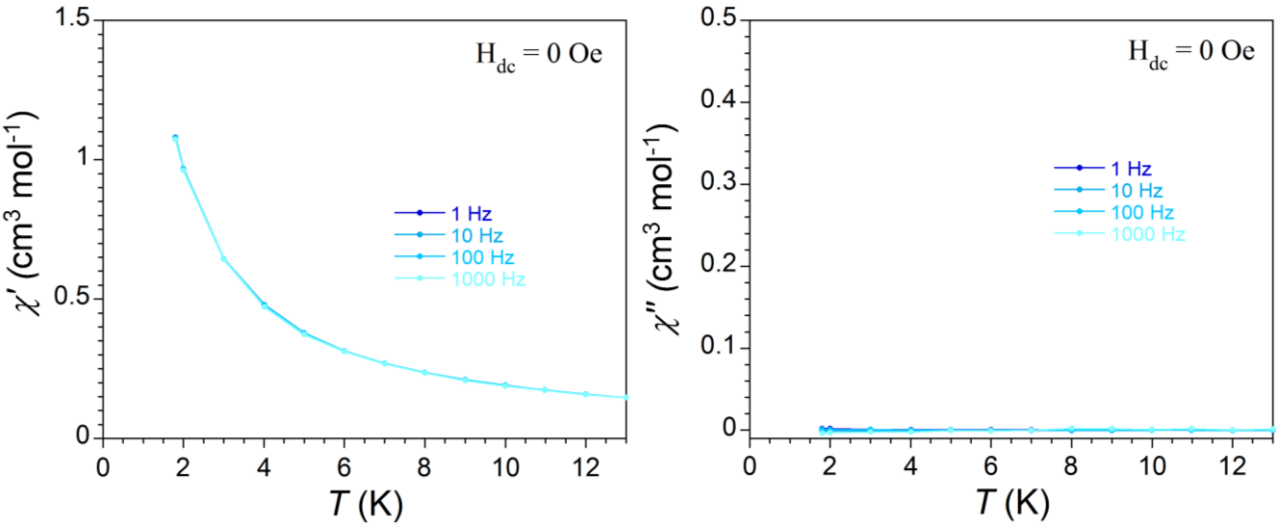

Figure S10: Temperature dependence of the in-phase (χ') and out-of-phase (χ'') ac magnetic susceptibility for **1** in zero Oe applied dc field at different ac frequencies between 1 and 1000 Hz and with a 4 Oe oscillating ac field. The lack of out of phase ac susceptibility signal signifies no slow dynamics of magnetization.

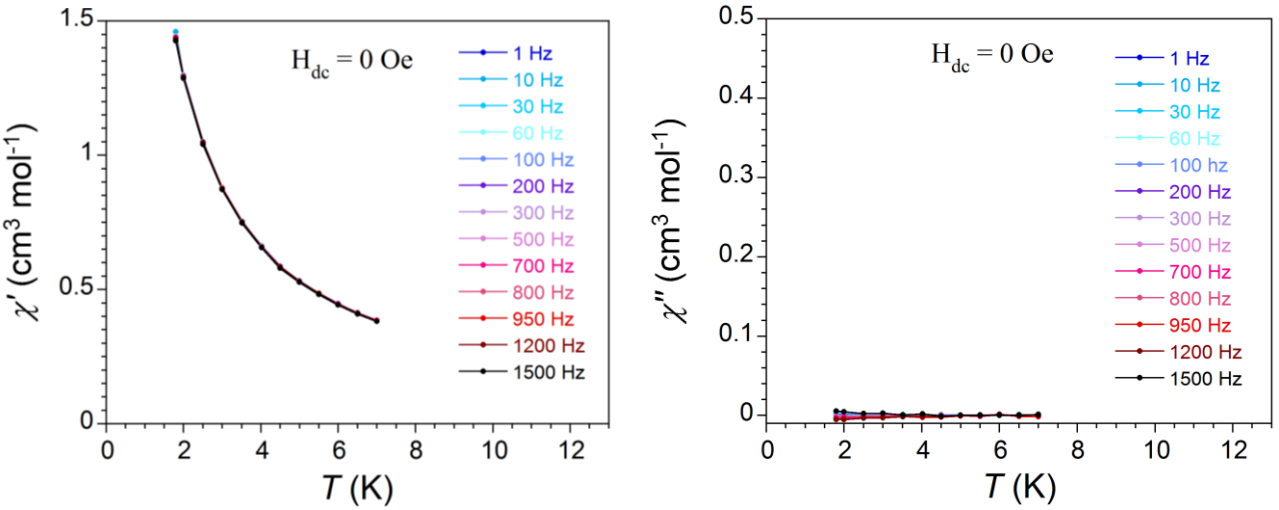

Figure S11: Temperature dependence of the in-phase (χ') and out-of-phase (χ'') ac magnetic susceptibility for **2** in zero Oe applied dc field at different ac frequencies between 1 and 1500 Hz and with a 4 Oe oscillating ac field. The lack of out of phase ac susceptibility signal signifies no slow dynamics of magnetization.

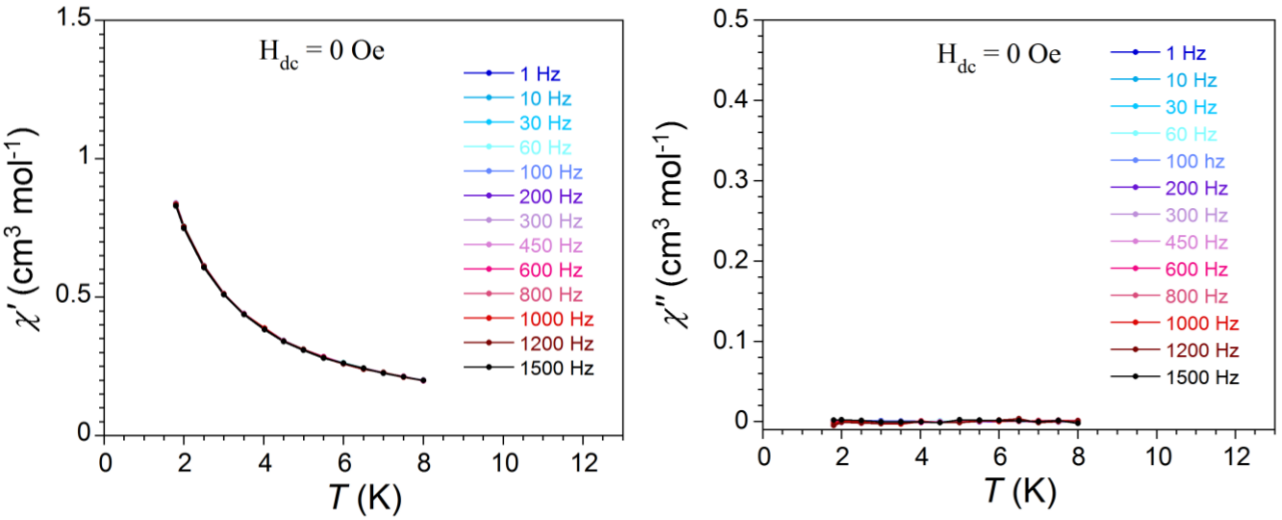

Figure S12: Temperature dependence of the in-phase (χ') and out-of-phase (χ'') ac magnetic susceptibility for **3** in zero Oe applied dc field at different ac frequencies between 1 and 1500 Hz and with a 4 Oe oscillating ac field. The lack of out of phase ac susceptibility signal signifies no slow dynamics of magnetization.

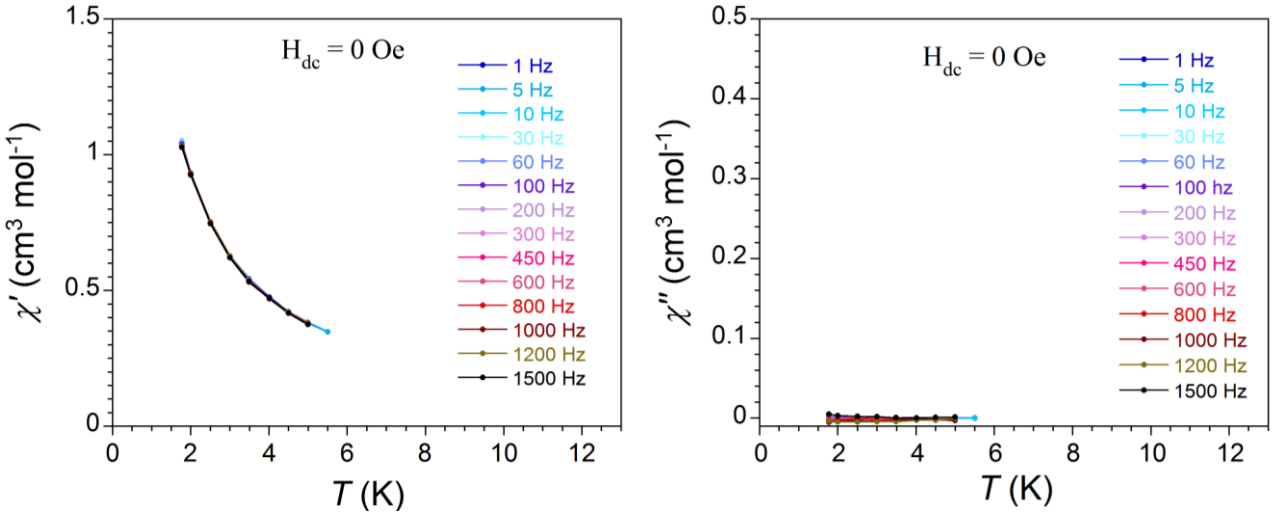

Figure S13: Temperature dependence of the in-phase (χ') and out-of-phase (χ'') ac magnetic susceptibility for **4** in zero Oe applied dc field at different ac frequencies between 1 and 1500 Hz and with a 4 Oe oscillating ac field. The lack of out of phase ac susceptibility signal signifies no slow dynamics of magnetization.

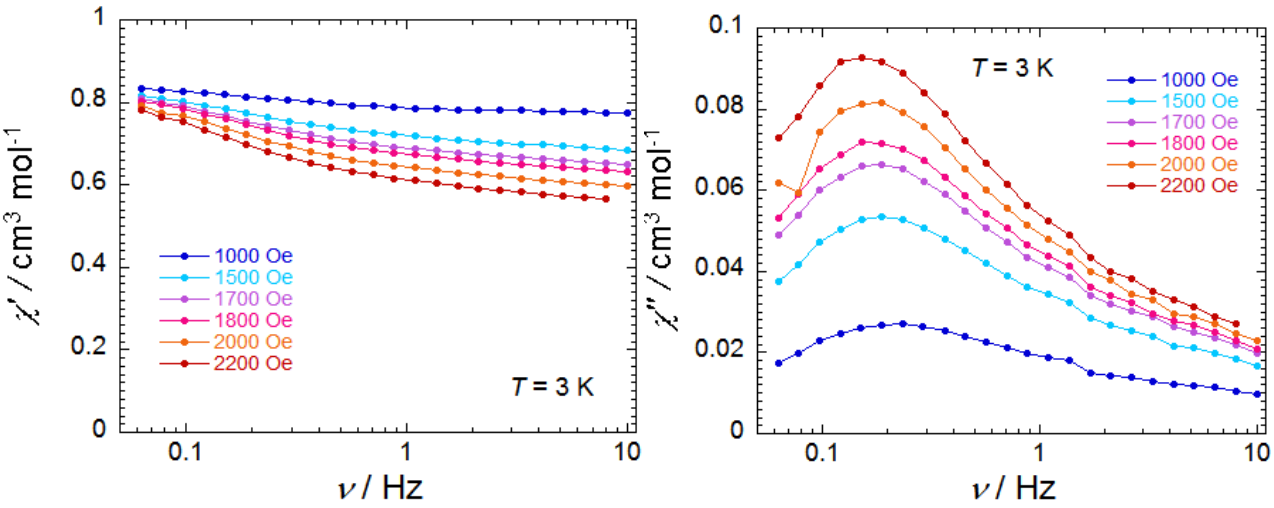

Figure S14: The frequency dependence of the in-phase (χ') and out-of-phase (χ'') ac magnetic susceptibility of **1a** at 3 K at different applied dc fields from 1000 to 2200 Oe and with a 4 Oe oscillating ac field.

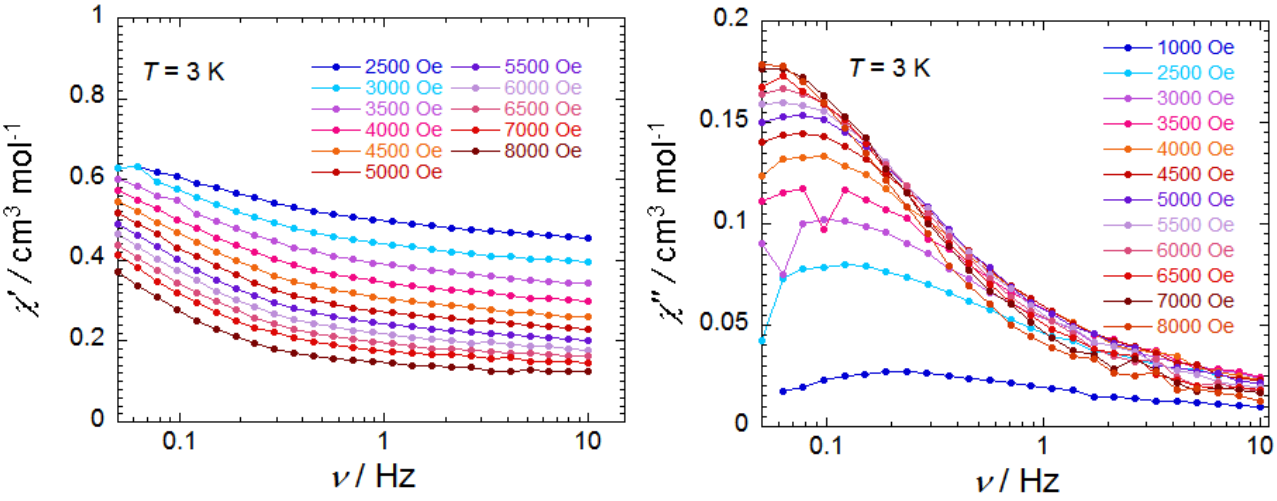

Figure S15: The frequency dependence of the in-phase (χ') and out-of-phase (χ'') ac magnetic susceptibility of **1a** at 3 K at different applied dc fields from 1000 to 8000 Oe and with a 4 Oe oscillating ac field.

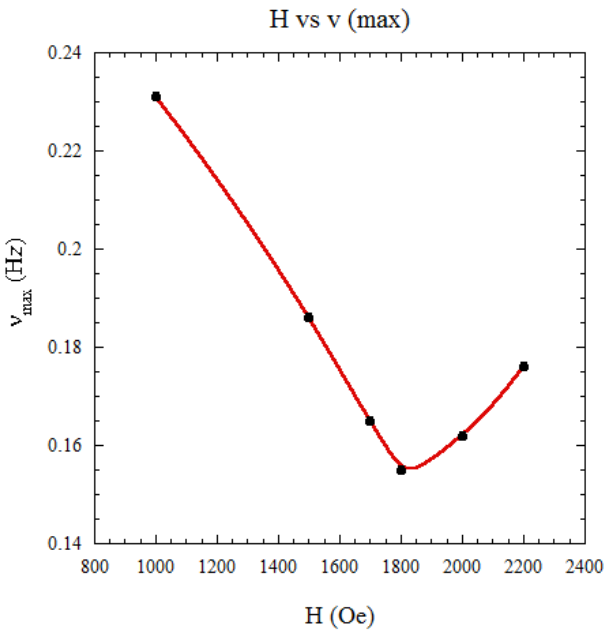

Figure S16: Field dependence of the characteristic relaxation frequency of the magnetization (ν_{max}) as a function of the applied field at 3 K for compound **1a**. This plot is deduced from the out-of-phase (χ'') ac magnetic susceptibility plot in Figure S15. It finds a minimum value at 1800 Oe indicating the slowest relaxation at that field. The solid line is a guide to the eye.

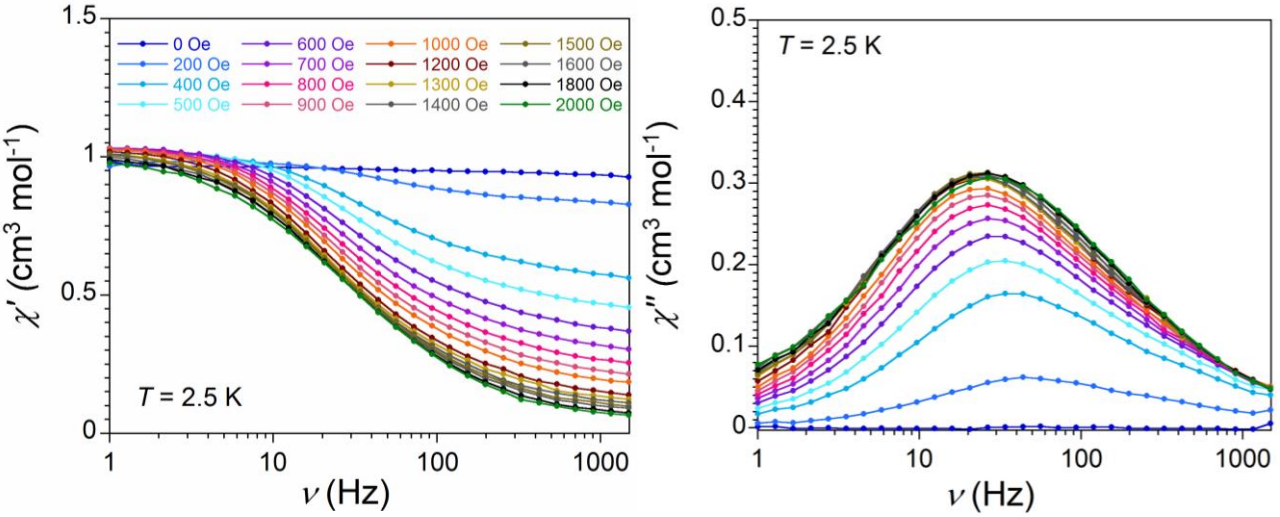

Figure S17: The frequency dependence of in-phase (χ') and out-of-phase (χ'') ac magnetic susceptibility of **1** at 2.5 K at different applied dc fields between zero and 2000 Oe and with a 4 Oe oscillating ac field.

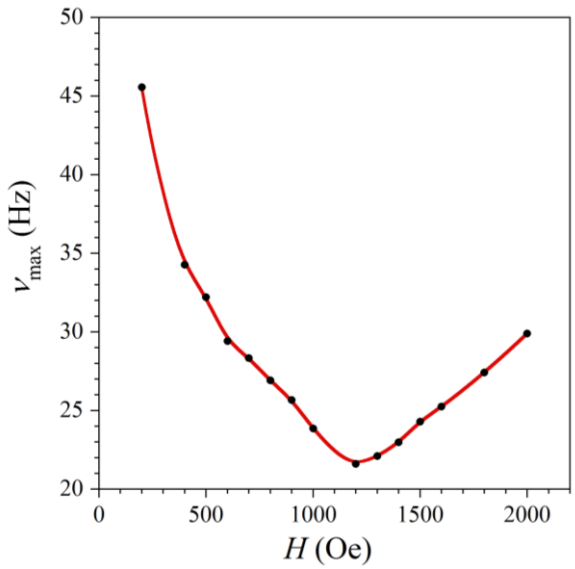

Figure S18: Field dependence of the characteristic relaxation frequency of the magnetization (ν_{max}) as a function of the applied field in **1** at 2.5 K. This plot is deduced from the out-of-phase (χ'') ac magnetic susceptibility plot in Figure S6. It finds a minimum value at 1200 Oe indicating the slowest relaxation at that field. The solid line is a guide to the eye.

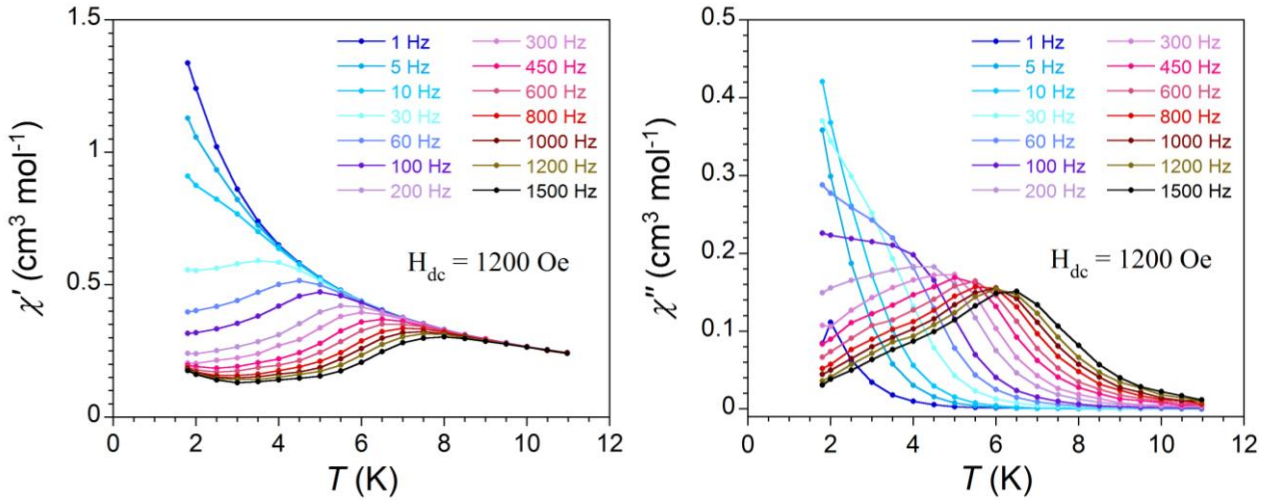

Figure S19: Temperature dependence of the in-phase (χ') and out-of-phase (χ'') ac magnetic susceptibility for **1** in 1200 Oe applied dc field at different ac frequencies between 1 and 1500 Hz and with a 4 Oe oscillating ac field. The presence of nonzero signal in the out of phase ac susceptibility signifies the slow dynamics of magnetization below 8 K.

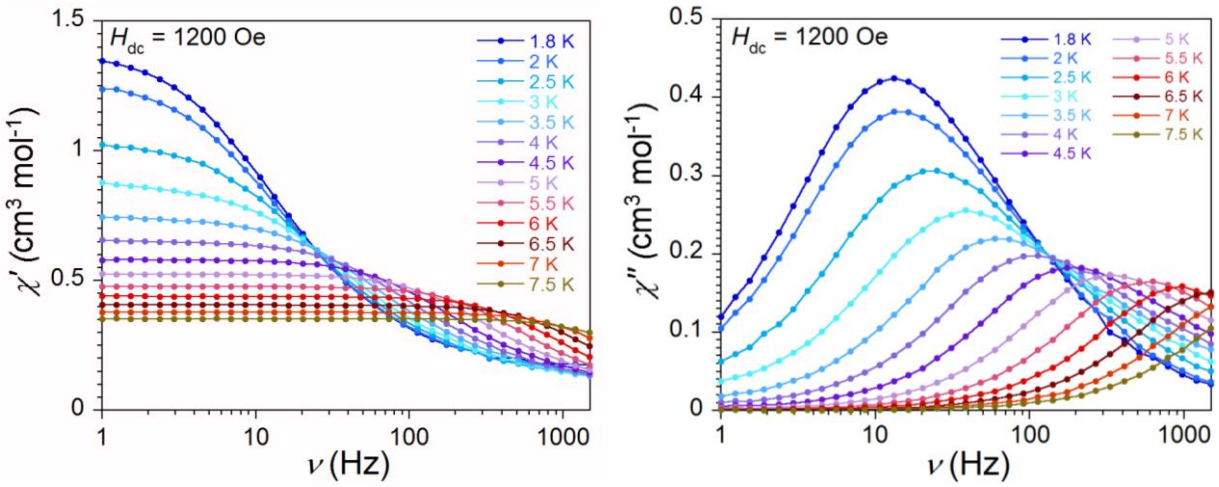

Figure S20: The frequency dependence of the in-phase (χ') and out-of-phase (χ'') ac magnetic susceptibility for **1** in 1200 Oe applied dc field and 4 Oe oscillating ac field at different temperatures.

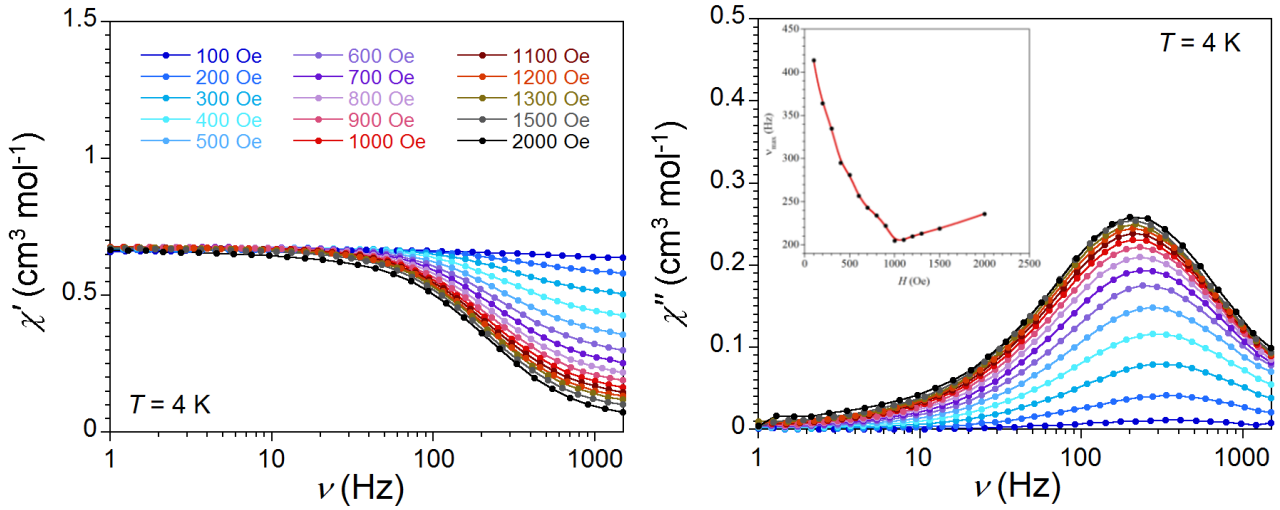

Figure S21: The frequency dependence of the in-phase (χ') and out-of-phase (χ'') ac magnetic susceptibility of **2** at 4 K at different applied dc fields between zero and 2000 Oe and with a 4 Oe oscillating ac field. Inset: Field dependence of the characteristic relaxation frequency of the magnetization (ν_{max}) as a function of the applied field. This plot is deduced from out-of-phase (χ'') ac magnetic susceptibility plot and it finds a minimum value at 1000 Oe indicating the slowest relaxation at that field. The solid line is a guide to the eye.

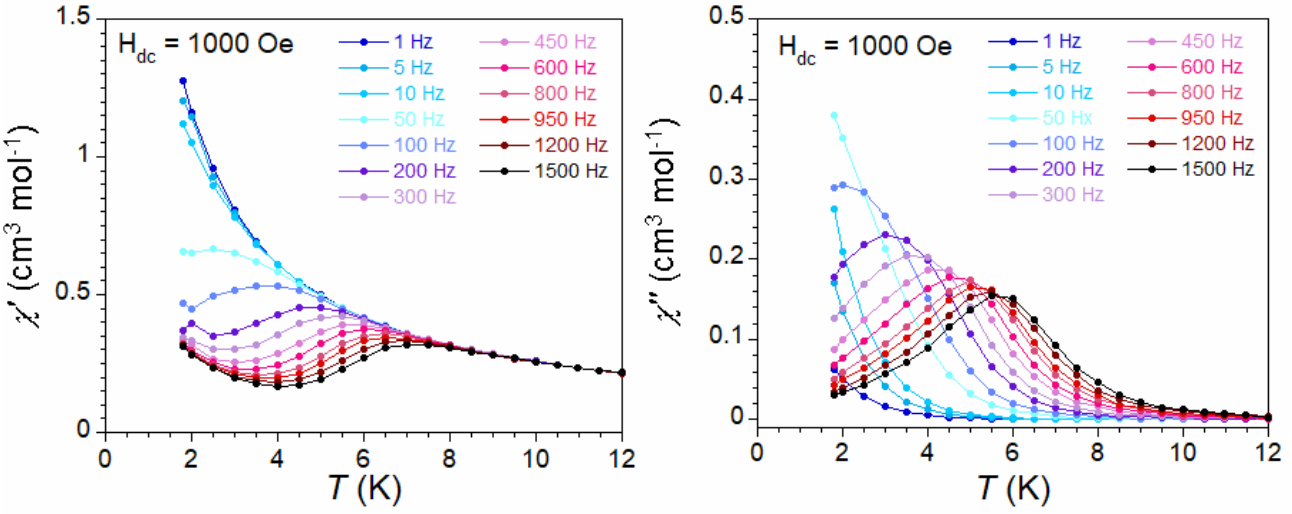

Figure S22: Temperature dependence of the in-phase (χ') and out-of-phase (χ'') ac magnetic susceptibility for **2** in 1000 Oe applied dc-field at different ac frequencies between 1 and 1500 Hz and with a 4 Oe oscillating ac field. The nature of ac susceptibility signifies slow dynamics of magnetization below 7 K.

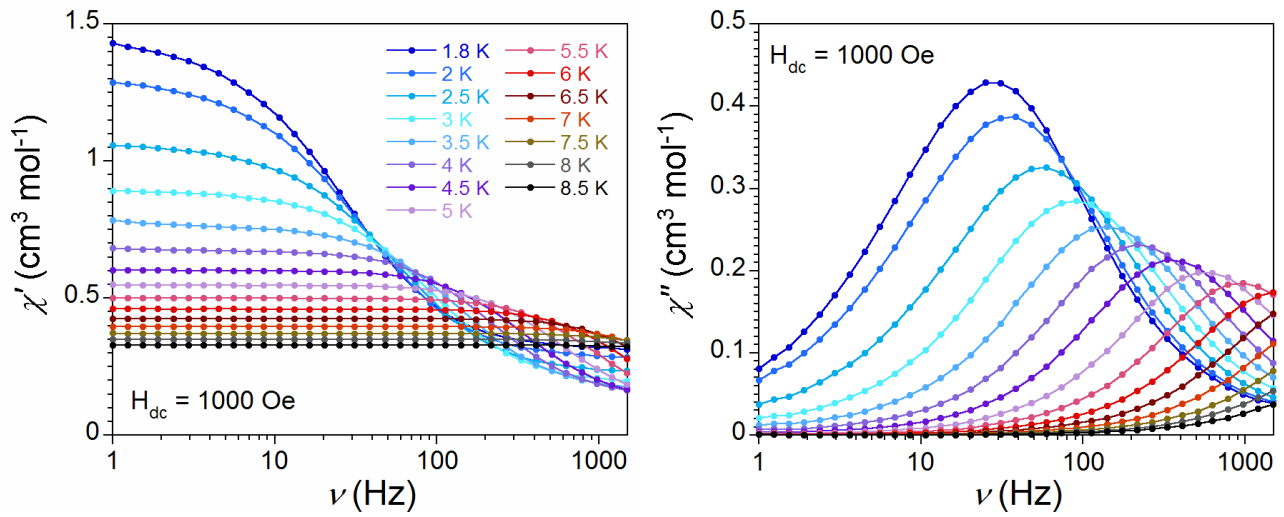

Figure S23: The frequency dependence of the in-phase (χ') and out-of-phase (χ'') ac magnetic susceptibility for **2** in 1000 Oe applied dc-field and 4 Oe oscillating ac field at different temperatures.

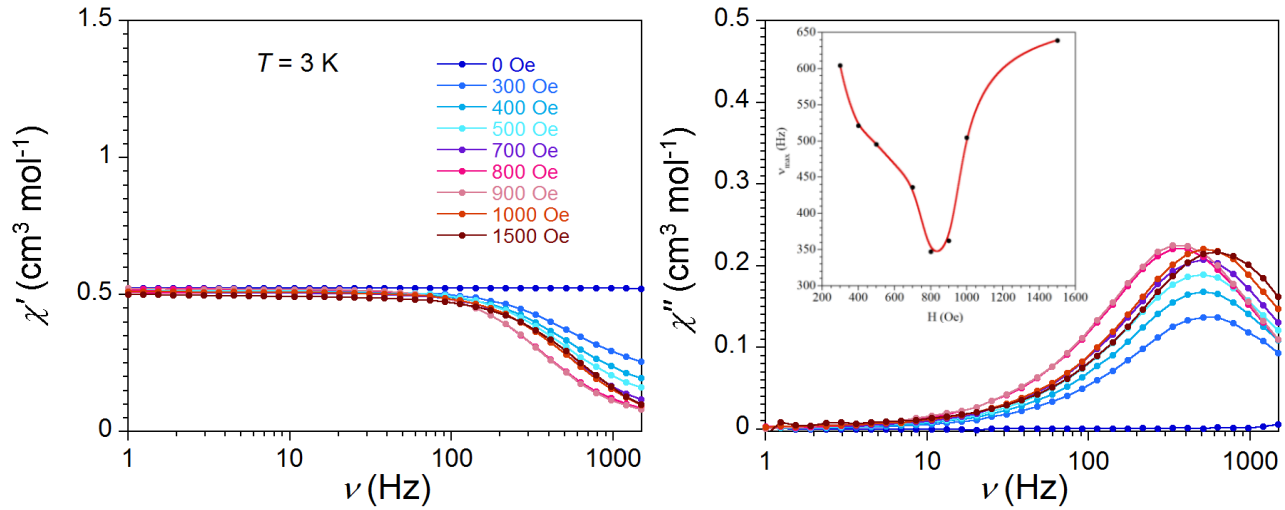

Figure S24: The frequency dependence of the in-phase (χ') and out-of-phase (χ'') ac magnetic susceptibility of **3** at 3 K at different applied dc fields between zero and 1500 Oe and with a 4 Oe oscillating ac field. Inset: Field dependence of the characteristic relaxation frequency of the magnetization (ν_{max}) as a function of the applied field. This plot is deduced from out-of-phase (χ'') ac magnetic susceptibility plot and it finds a minimum value at 800 Oe indicating the slowest relaxation at that field. The solid line is a guide to the eye.

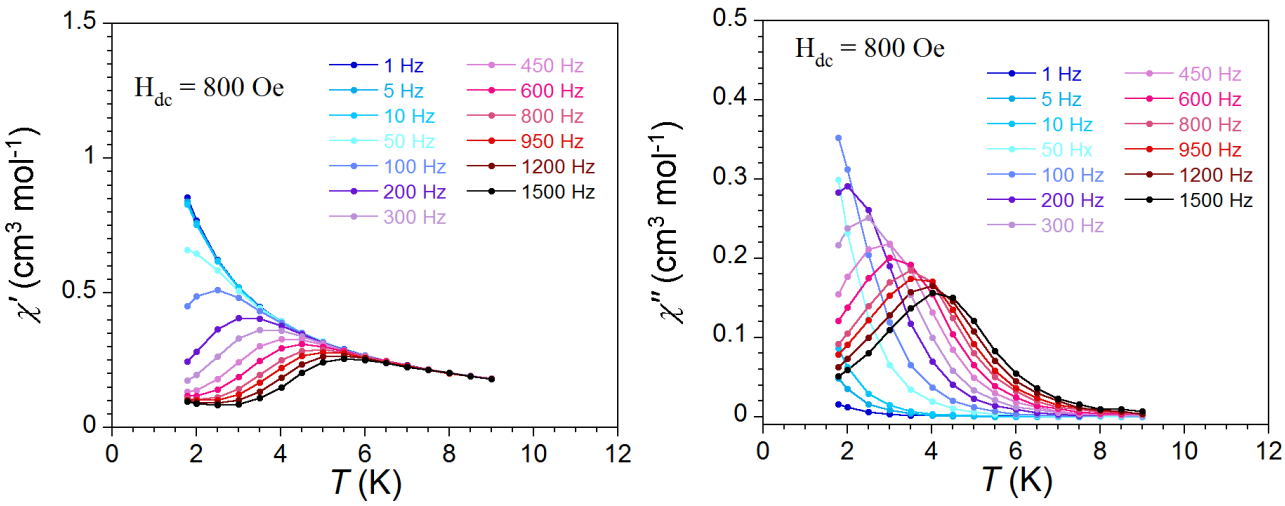

Figure S25: Temperature dependence of the in-phase (χ') and out-of-phase (χ'') ac magnetic susceptibility for **3** in 800 Oe applied dc-field at different ac frequencies between 1 and 1500 Hz and with a 4 Oe oscillating ac field. The nature of ac susceptibility signifies the slow dynamics of magnetization below 5.5 K.

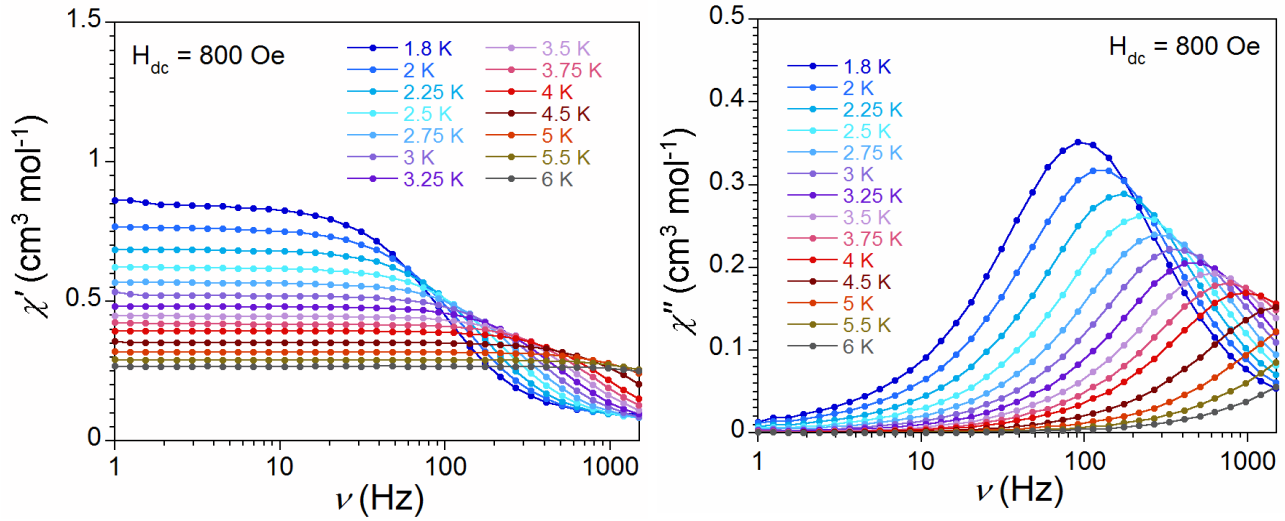

Figure S26: The frequency dependence of the in-phase (χ') and out-of-phase (χ'') ac magnetic susceptibility for **3** in 800 Oe applied dc field and 4 Oe oscillating ac field at different temperatures.

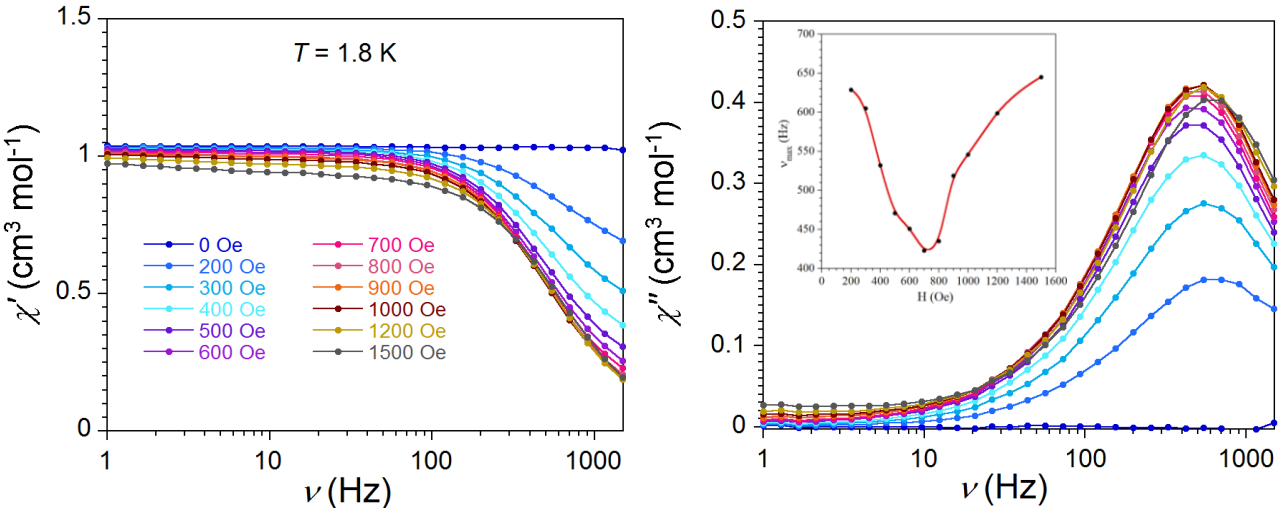

Figure S27: The frequency dependence of the in-phase (χ') and out-of-phase (χ'') ac magnetic susceptibility of **4** at 1.8 K at different applied dc fields between zero and 1500 Oe and with a 4 Oe oscillating ac field. Inset: Field dependence of the characteristic relaxation frequency of the magnetization (ν_{max}) as a function of the applied field. This plot is deduced from out-of-phase (χ'') ac magnetic susceptibility plot and it finds a minimum value at 700 Oe indicating the slowest relaxation at that field. The solid line is a guide to the eye.

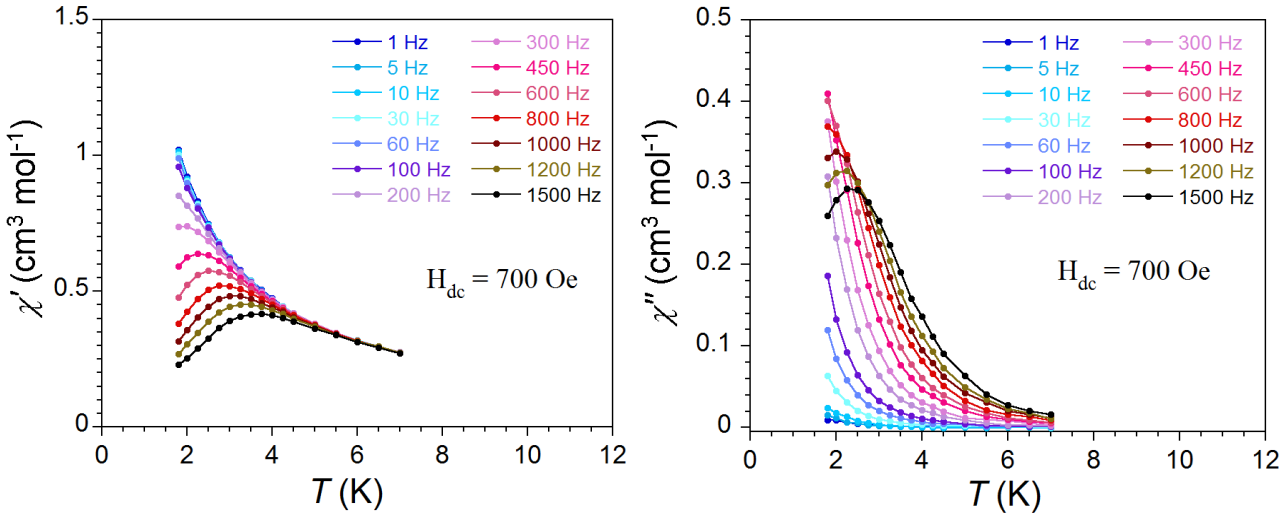

Figure S28: Temperature dependence of the in-phase (χ') and out-of-phase (χ'') ac magnetic susceptibility for **4** in 700 Oe applied dc field at different ac frequencies between 1 and 1500 Hz and with a 4 Oe oscillating ac field. The nature of ac susceptibility signifies the slow dynamics of magnetization below 4 K.

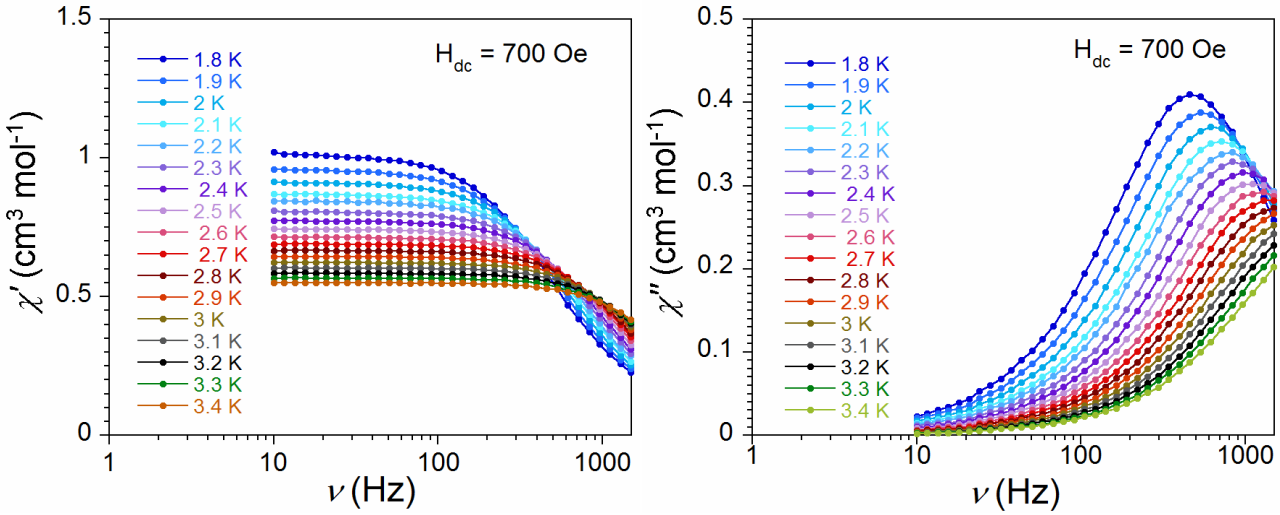

Figure S29: The frequency dependence of the in-phase (χ') and out-of-phase (χ'') ac magnetic susceptibility for **4** in 700 Oe applied dc field and 4 Oe oscillating ac field at different temperatures.

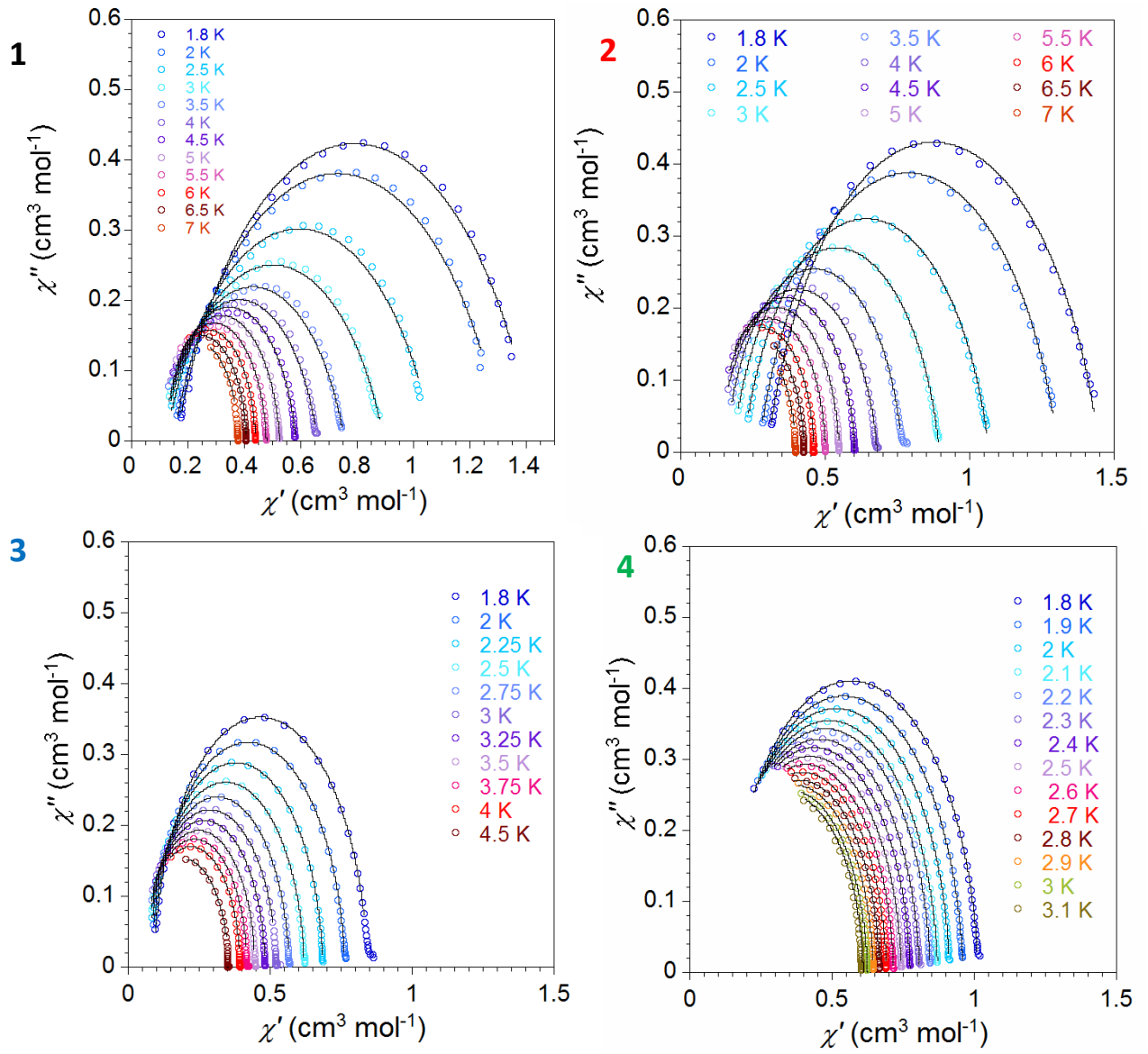

Figure S30: Cole-Cole plots for compounds **1-4**.

Note for Cole-Cole plots: At fixed temperatures between 1.8 and 7 K (for **1** and **2**), 1.8 and 4.5 K (for **3**) and 1.8 and 3.1 K (for **4**), semicircle Cole-Cole plots of $\chi'(\nu)$ vs $\chi''(\nu)$ were generated and fitted using the generalized Debye model considering a single relaxation pathway (Fig. S30). The α parameter which is the measure of the distribution of relaxation times, ranges between 0.238-0.027 (for **1**), 0.174-0.013 (for **2**), 0.052-0.016 (for **3**) and 0.044-0.008 (for **4**) indicating that the distribution pattern of single relaxation processes changes significantly with the change of ligand environment of Co(II). Compounds **1** and **2** have a large range of α parameter, indicating wider distribution of relaxation times compared to compounds **3** and **4**. Additionally the low temperature (below 4 K) of $\tau(T)$ vs. T^{-1} data of **1** and **2** possess a larger deviation from the linear behaviour which are typically attributed to the quantum tunnelling of magnetization (QTM) which is visually less contributing in the relaxation of **3** and **4**. The wider distribution of α parameter in the Cole-Cole plot of **1** and **2** at lower temperatures also supports the present of more QTM mechanism associate in the low temperature relaxation mechanism.

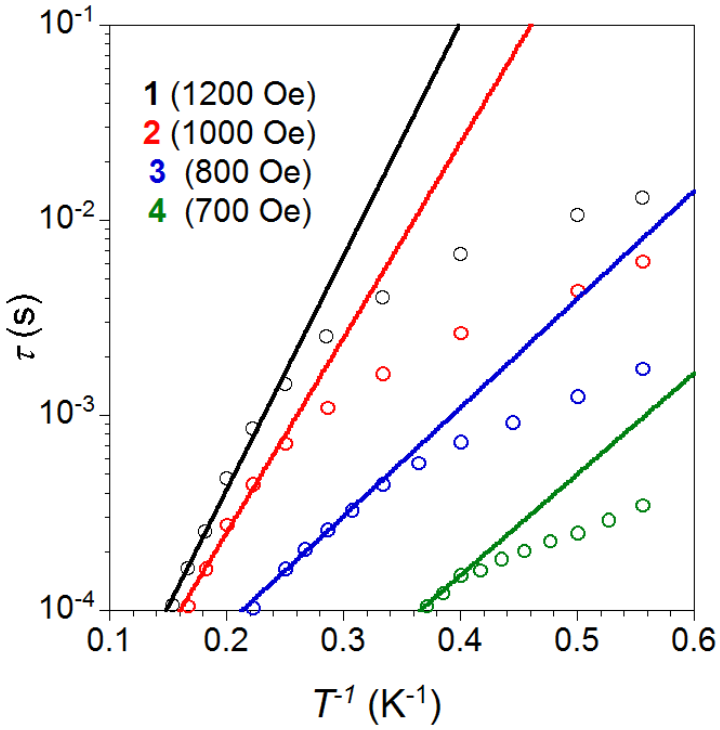

Figure S31: Semi log plots of $\tau(T)$ vs. $1/T$ for compounds **1-4**. Solid lines are the best fits to the Arrhenius law (Orbach relaxation) for the linear part of the relaxation time, with the equation $\tau(T) = \tau_0 \exp(U_{eff}/k_B T)$, detail as discussed in the main text.

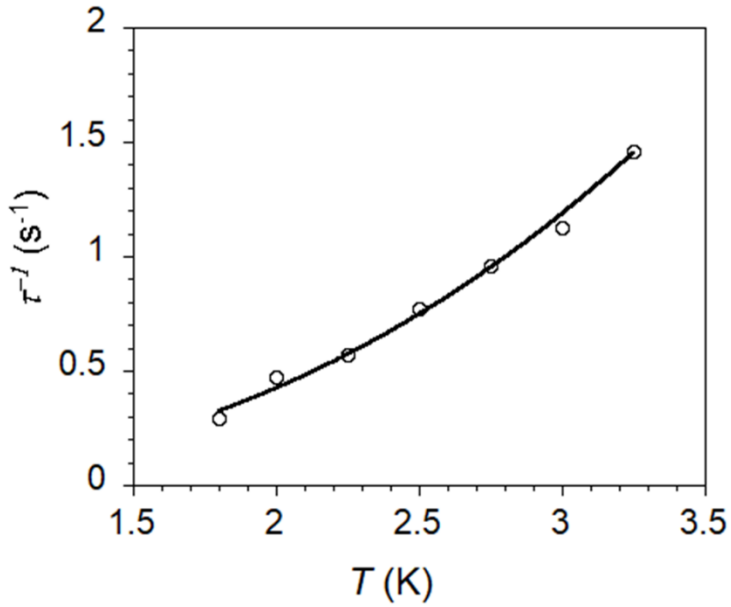

Figure S32: The fit of τ^{-1} vs T data of **1a** with power law $\tau^{-1} = bT^n$. The polynomial exponent n = 2.54 with matrix coefficient b = 0.073 (R = 0.9964). The value of n ≈ 2 indicates possible presence of phonon bottleneck mechanism.

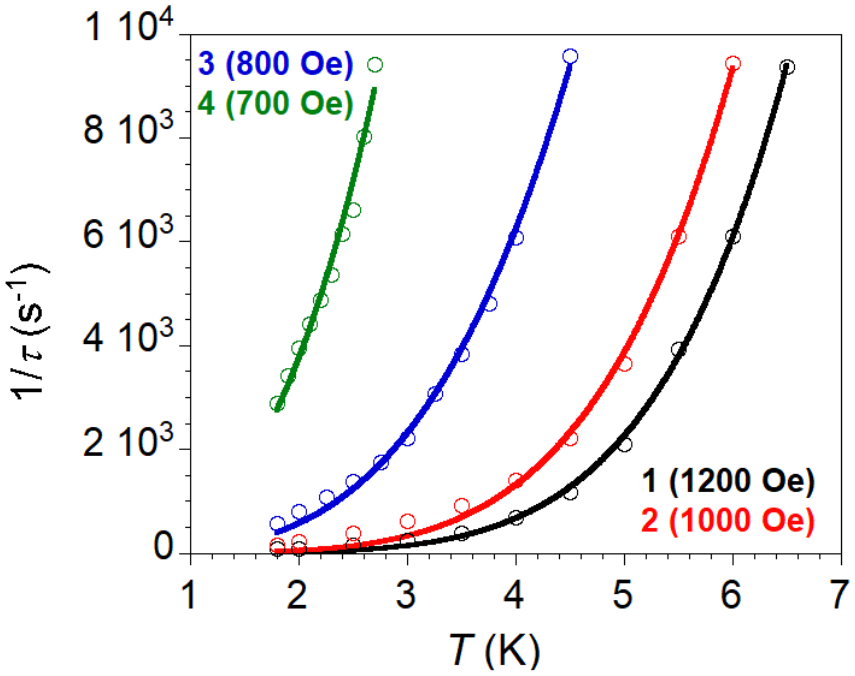

Figure S33: The fit of τ^{-1} vs T data of compounds **1-4** with Raman relaxation mechanism using the equation $\tau^{-1} = bT^n$, *n* is the power exponent of the temperature dependence of the relaxation time, *b* is the coefficient of Raman relaxation.

AOM analysis:

Compound
1 $Co^{II}(H_2bip)_2Cl_2$
2 $Co^{II}(H_2bip)_2Br_2$
3 $[Co^{II}(H_2bip)_3](Br)_2$
4 $[Co^{II}(H_2bip)_2(4,4'Me\text{-}2,2'bipy)](Br)_2$

$e_\sigma(Cl) = 3000\ cm^{-1}$
$e_\sigma(Br) = 2500\ cm^{-1}$
$e_\sigma(N_{imine}) = 3500\ cm^{-1}$
$e_\sigma(N_{bipy}) = 4500\ cm^{-1}$
$e_\pi(Cl) = 600\ cm^{-1}$
$e_\pi(Br) = 300\ cm^{-1}$
$e_\pi(N_{imine}) = 100\ cm^{-1}$
$e_\pi(N_{bipy}) = -500\ cm^{-1}$

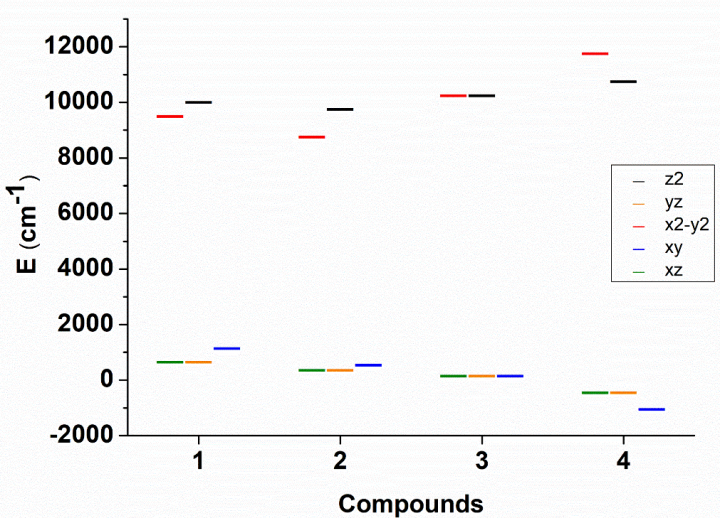

Compounds	z^2 (cm^{-1})	x^2-y^2 (cm^{-1})	xz (cm^{-1})	yz (cm^{-1})	xy (cm^{-1})
1	10250	9750	900	900	1400
2	10000	9000	600	600	800
3	10500	10500	400	400	400
4	11000	12000	-200	-200	-800

The rearrangement method of the *D* and *E* parameters:
Finding the E and D values greater than 1/3 is not unusual in many systems, and we have recalculated it based on reference S9: R. Boča, Theoretical Foundations of Molecular magnetism, Elsevier, 1999, pages 424-425. The calculation for compound 1 and 2 here:

Application to compound 1:
From PHI (Ref 23: N. F. Chilton, R. P. Anderson, L. D. Turner, A. Soncini and K. S. Murray, *J. Comput. Chem*., 2013, 34, 1164-1175)

D = - 66.68, *E* = 35.76. Now using these values,

$D = {}^{1}/_{2}\ (-D'_{xx} - D'_{yy} + 2D_{zz})$ and $E = {}^{1}/_{2}\ (D'_{xx} - D'_{yy})$. Therefore

$D'_{zz} = {}^{2}/_{3}\ D$ = - 44.45

$D'_{yy} = -{}^{1}/_{3}\ D - E$ = - 13.53

$D'_{xx} = -{}^{1}/_{3}\ D + E$ = 57.99

Now rearranging the *D* tensors as |*D*'zz|≥ |*D*'yy|≥ |*D*'xx| we find |57.99| > |44.45| > |13.53|

Therefore, the new $D = {}^{3}/_{2}\ D'_{zz} = {}^{3}/_{2} \times 57.99 = 86.98$ and new $E = {}^{1}/_{2}\ (D'_{xx} - D'_{yy}) = 15.46$.

So the *E/D* = 15.46/86.98 = 0.178

Application to compound 2:
From PHI (Ref 23: N. F. Chilton, R. P. Anderson, L. D. Turner, A. Soncini and K. S. Murray, *J. Comput. Chem*., 2013, 34, 1164-1175)

D = - 72.62, *E* = 34.21. Now using these values,

$D = {}^{1}/_{2}\ (-D'_{xx} - D'_{yy} + 2D_{zz})$ and $E = {}^{1}/_{2}\ (D'_{xx} - D'_{yy})$. Therefore

$D'_{zz} = {}^{2}/_{3}\ D$ = - 48.41

$D'_{yy} = -{}^{1}/_{3}\ D - E$ = -10.00

$D'_{xx} = -{}^{1}/_{3}\ D + E$ = 58.42

Now rearranging the *D* tensors as |*D*'zz|≥ |*D*'yy|≥ |*D*'xx| we find |58.42| > |48.41| > |10.00|

Therefore, the new $D = {}^{3}/_{2}\ D'_{zz} = {}^{3}/_{2} \times 58.42 = 87.63$ and new $E = {}^{1}/_{2}\ (D'_{xx} - D'_{yy}) = 19.21$.

So the *E/D* = 19.21/87.63 = 0.219.

Additional attempts to fit the static magnetic property data of compounds 1-4:

The susceptibility data were fit along with reduced field magnetization, using PHI,[S7] to spin Hamiltonians containing one magnetic centre, and best-fit parameters are listed in Table S1 below (third line, blue values). When only the *M* vs *H*/*T* data are fit with PHI[S7] (second line, red values in Table S1) and ANISOFIT[S8] (first line, black values in Table S1, Fig. S9), we find slightly different but comparable anisotropic parameters. The small differences of the *D* and *E* parameters found via PHI and ANISOFIT appear to be related to differences of the spin Hamiltonian formalisms. Interestingly, the *D* values obtained from the magnetization data (black and red lines in Table S1) show a positive sign of *D* for the compounds **1** and **2**, where the sign of *D* remains the same (see the blue line in Table S1) for compounds **3** and **4**. Note that the sign of *D* cannot be determined reliably from fits of magnetization data of a bulk sample. We find the $|D|$ of **1** obtained from *M* vs *H*/*T* fit (black and red lines in Table S1) is noticeably high but comparable to other compounds. In contrast, the *E* values are significantly large for **3** and **4** determined from the fit of the *M* vs *H*/*T* (black and red line in Table S1). Despite the variation of the fitting parameters collected in Table 2 in the article, an apparent decreasing trend in axiality (*D*) is found from **1-4**, where $|E/D|$ decreases. From the above discussion and the fitting parameters collected in Table 2 it is evident that magnetic data of the bulk Co(II)-molecular samples could be qualitatively sufficient to determine anisotropic parameters, but not sufficient for quantitative analysis.

Table S1. Fitting parameters of static magnetic properties for 1-4: *M* vs *H*/*T* using ANISOFIT (top line in black) and PHI (middle line in red); combined fits of $\chi_M T$ *vs T* and *M* vs *H*/*T* data using PHI (bottom line in blue). *D* and *E* in cm^{-1}

	g	***D*[a]**	**$\|E\|$**	**$\|E/D\|$**	**R^2**
1	2.92	+115.0	31.0	0.269	
	2.93	+117.30	34.02	0.293*	99.9811
	2.62, 3.13	+86.98*	15.46*	0.178*	99.9999
2	2.96	+81.5	19.2	0.236	
	3.01	+86.39	21.60	0.250*	99.9091
	2.63, 3.09	+87.63*	19.21*	0.219*	99.9985
3	2.53	-24.9	5.3	0.213	
	2.52	-24.86	5.12	0.206	99.5968
	2.54, 2.91	-21.68	0.16	0.007	99.9307
4	2.59	+65.5	13.5	0.206	
	2.57	+64.50	13.42	0.208*	99.9867
	2.96, 2.33	+77.53	0.30	0.004	99.9821

[a] Note that the sign of *D* cannot be determined reliably from fits to magnetic susceptibility or magnetization data of a bulk sample.

* The *E*/*D* values are recalculated using the rearrangement of the D_{xx}, D_{yy} and D_{zz} parameters according to reference S9.

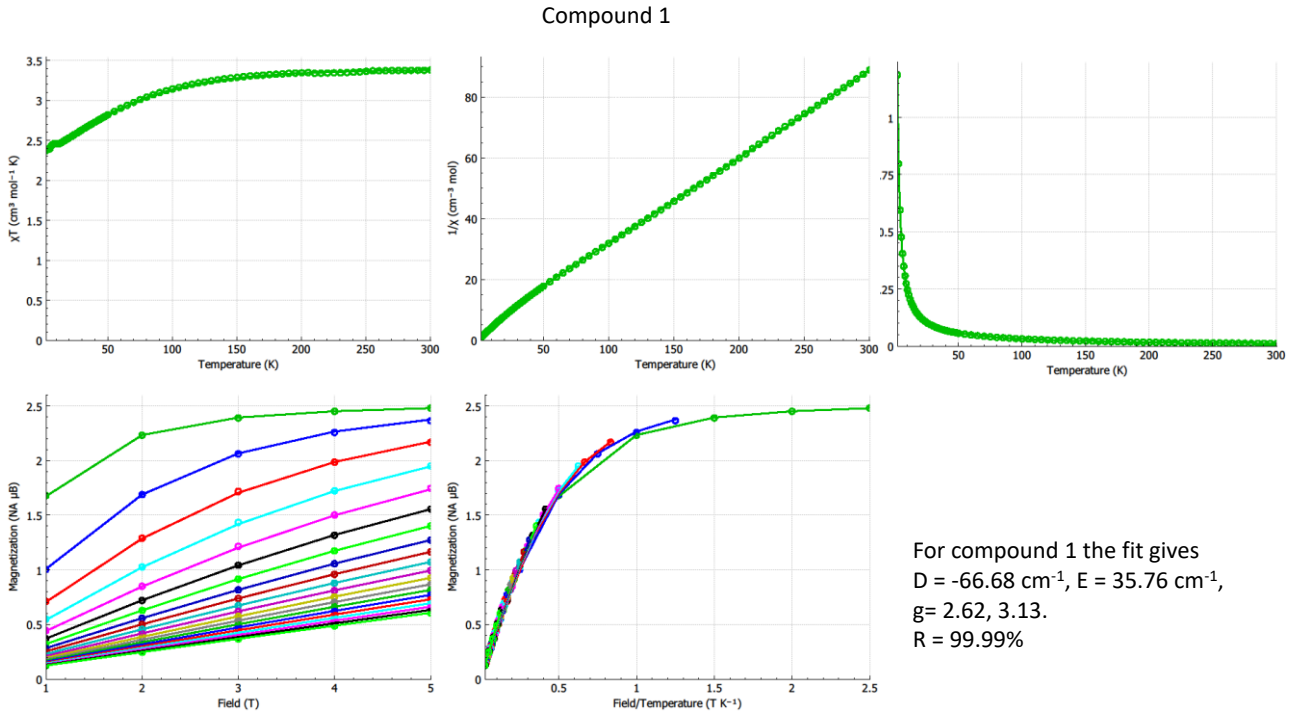

Figure S34: The fit of the $\chi_M T$ vs T and M vs H/T data of compound **1** using PHI[S7] which determines D = -66.68 cm^{-1}, E = 35.76 cm^{-1}. The rearranged D and E, and g values are listed in blue in the table S1. The rearrangement method of the D and E parameters is described above.

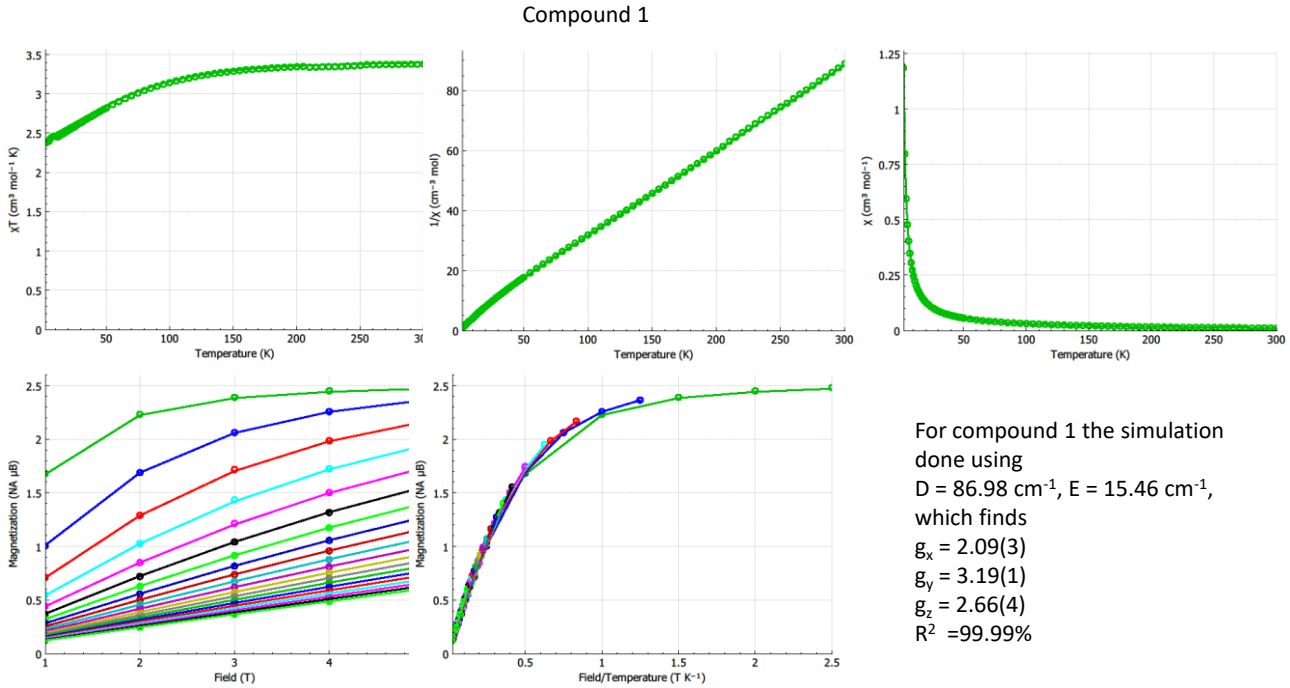

Figure S35: The simulation of the $\chi_M T$ vs T and M vs H/T data of compound **1** using fixed D and E values which gives new g_x, g_y, and g_z values. We have used PHI for the simulation.[S7] The D, E and g values are listed in the table 2 of the main manuscript.

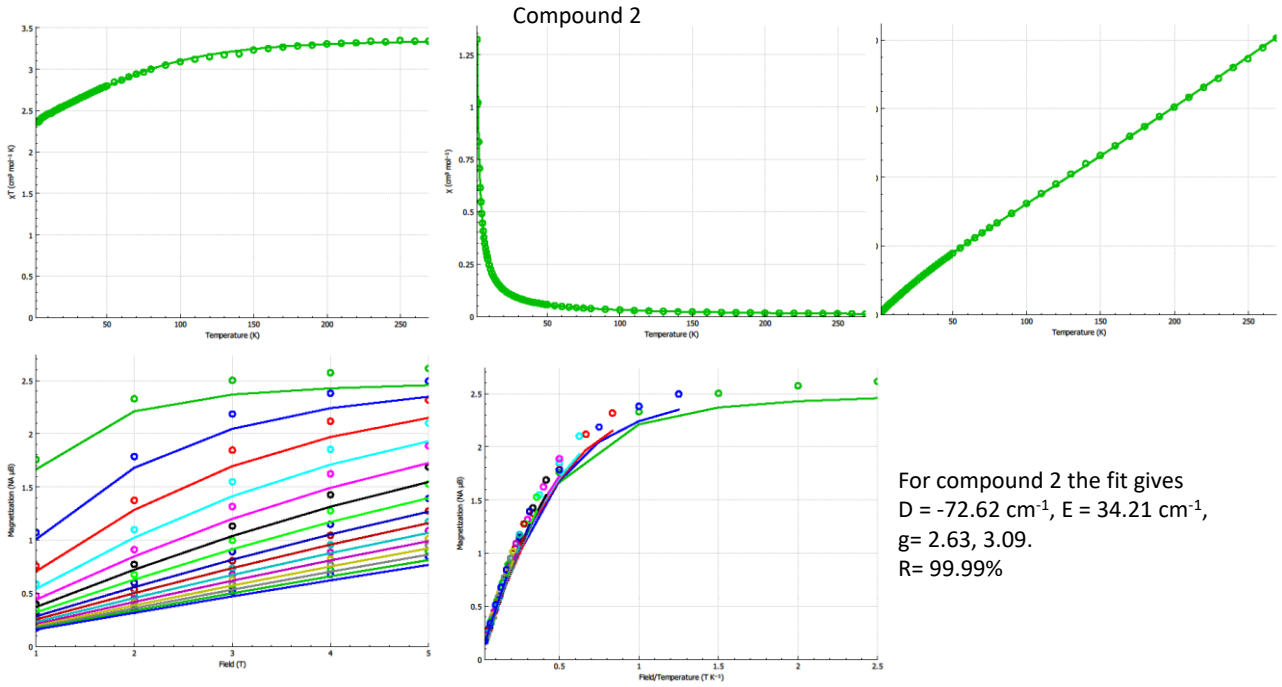

Figure S36: The fit of the $\chi_M T$ vs T and M vs H/T data of compound **2** using PHI[S7] which determines D = -72.62 cm^{-1}, E = 34.21 cm^{-1}. The rearranged D and E, and g values are listed in blue in the table S1. The rearrangement method of the D and E parameters is described above.

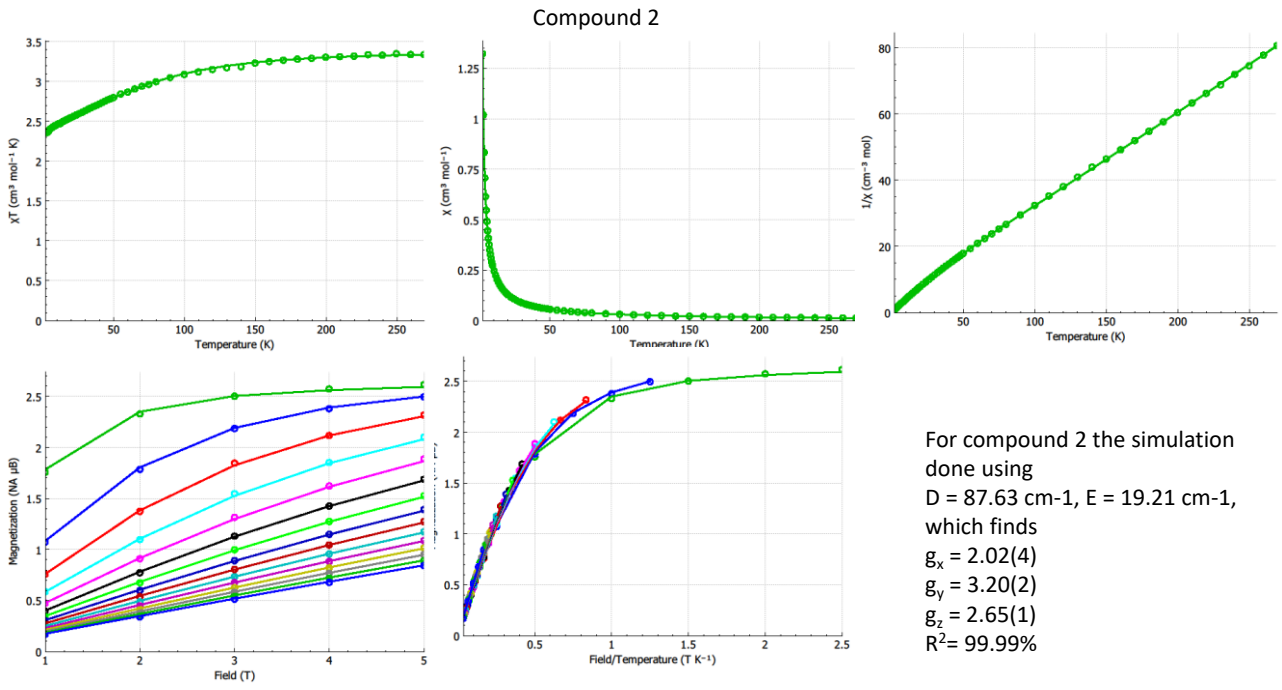

Figure S37: The simulation of the $\chi_M T$ vs T and M vs H/T data of compound **2** using fixed D and E values which gives new g_x, g_y, and g_z values. We have used PHI for the simulation.[S7] These values are listed in the table 2 of the main manuscript.

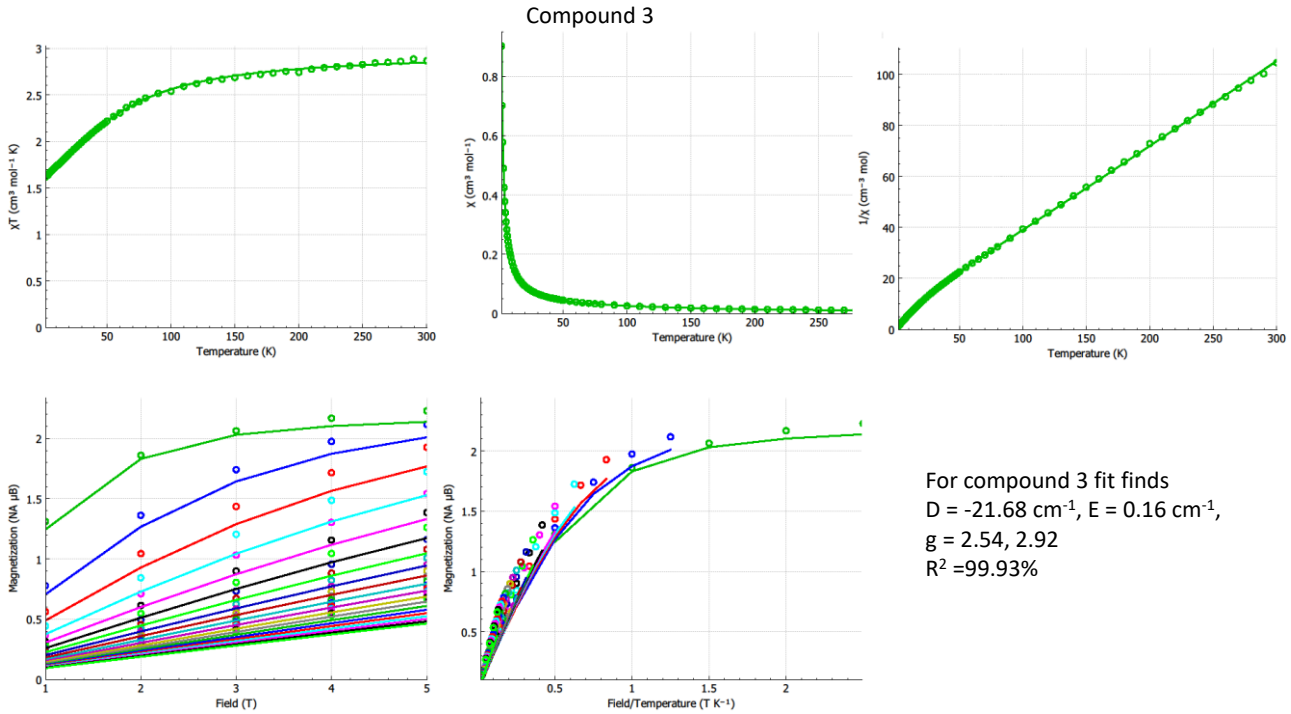

Figure S38: The fit of the $\chi_M T$ vs T and M vs H/T data of compound **3** using PHI[S7] which determines D = -21.68 cm^{-1}, E = 0.16 cm^{-1}. The D, E and g values are listed in the table 2 of the main manuscript.

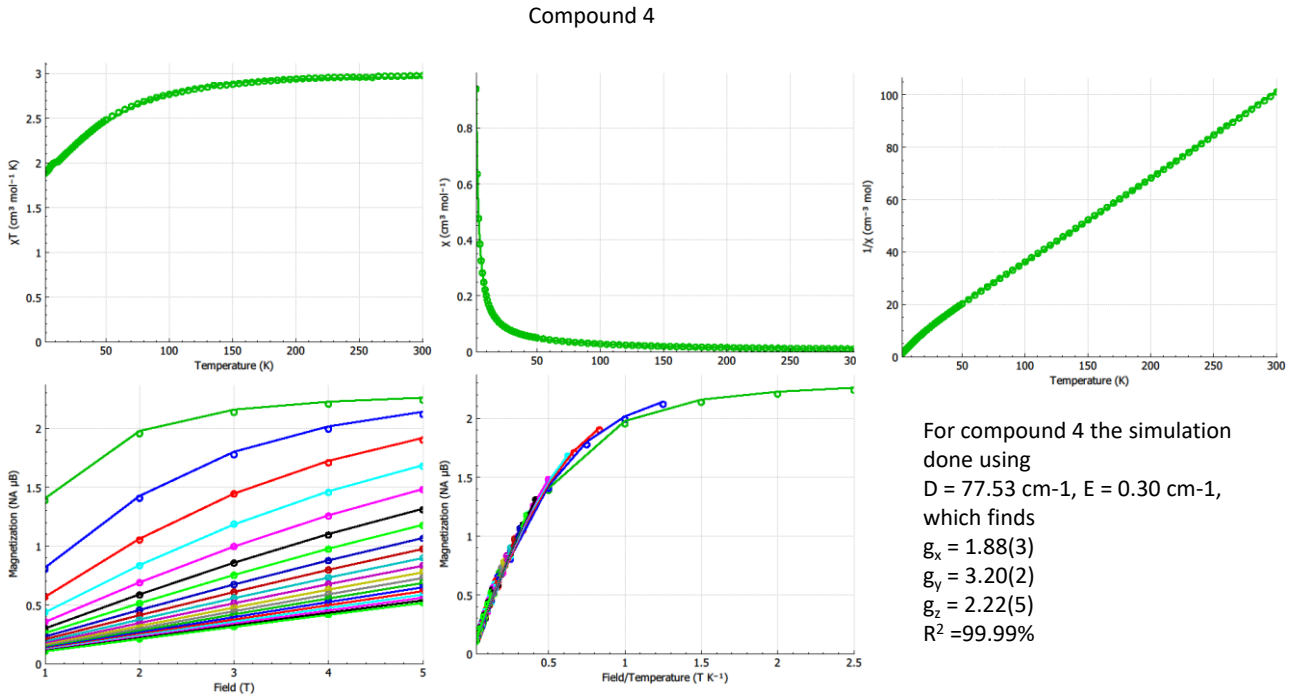

Figure S39: The simulation of the $\chi_M T$ vs T and M vs H/T data of compound **4** using fixed D and E values which gives new g_x, g_y, and g_z values. We have used PHI for the simulation.[S7]. The D, E and g values are listed in the table 2 of the main manuscript.

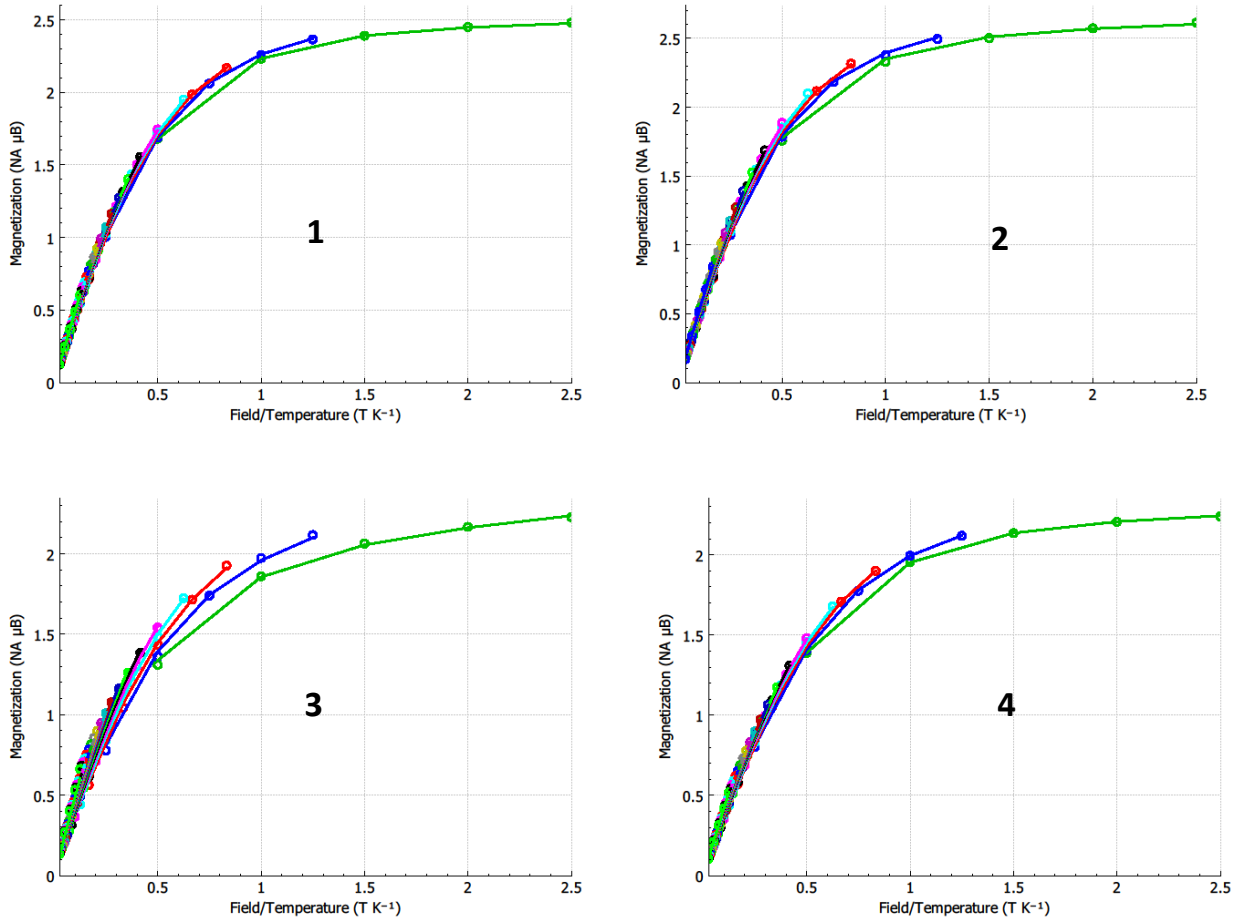

Figure S40: The fit of the only *M* vs *H*/*T* data of compounds **1-4** using PHI[S7]. The corresponding *D*, *E* and *g* parameters are listed in red coloured data in the Table S1.

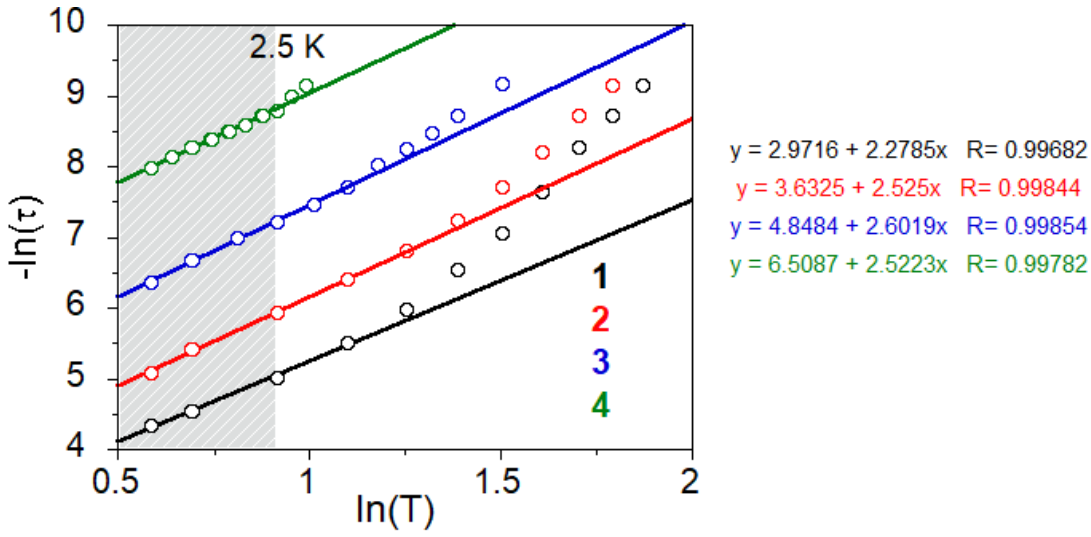

Figure S41: The linear fit of the ln(*τ*) vs ln(*T*) data of compounds **1-4** at low temperature (below ~ 2.5 K). The intercept and the slope of the fit represents the *b* and *n* of the Raman like relaxation for the equation $\tau^{-1} = bT^n$.

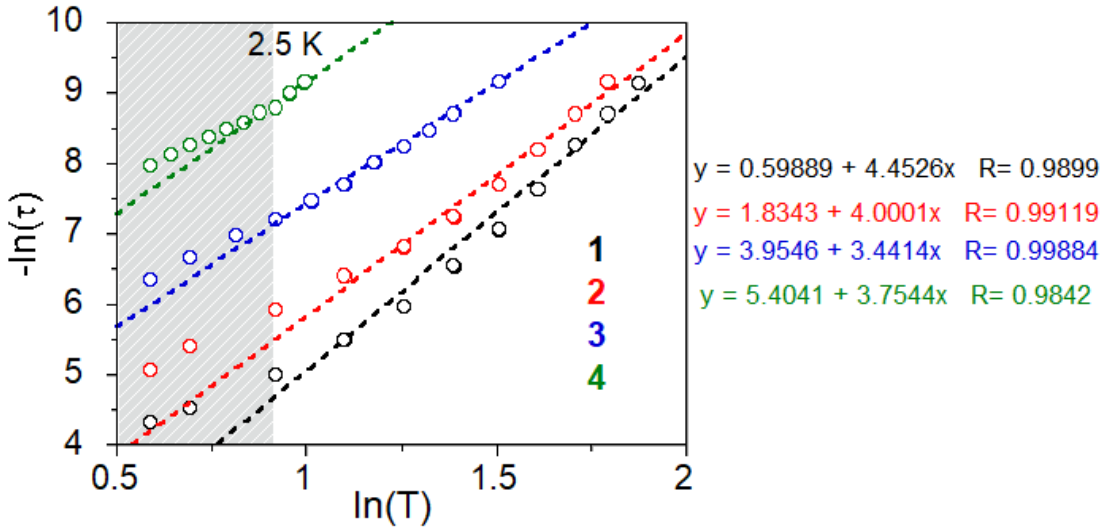

Figure S42: The linear fit of the ln(τ) vs ln(T) data of compounds **1-4** at higher temperature (above~ 2.5 K). The intercept and the slope of the fit represents the b and n of the Raman like relaxation for the equation $\tau^{-1} = bT^n$.

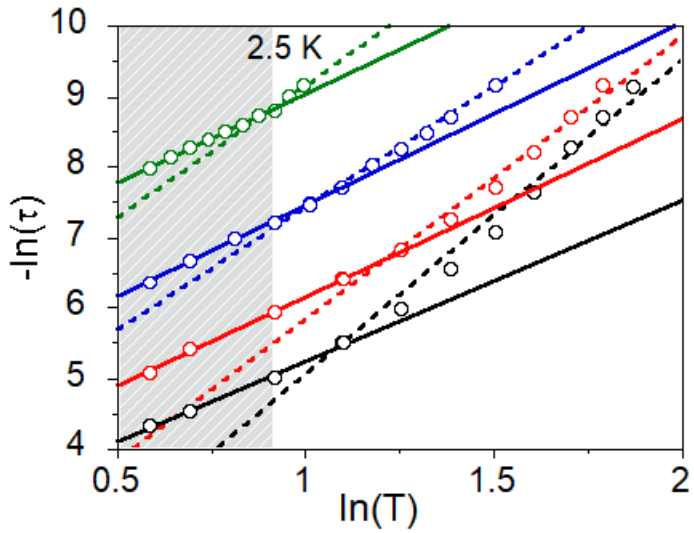

Figure S43: The linear fit of the ln(τ) vs ln(T) data of compounds **1-4** separately below and above ~ 2.5 K. It shows that at low temperature may be one type of phonon are driving the slow magnetic dynamics in all four compounds, but as the temperature increase near 3 K the magnetic dynamics are varied compound to compound, which could be Raman-like with different phonons or exponential (as in figure S31).

Table S2: Magnetic relaxation parameters for compounds **1-4** analysed with different mechanisms					
	Parameters	**1**	**2**	**3**	**4**
dc field	H_{dc} (Oe)	1200	1000	800	700
τ@1.8K	τ (1.8 K) in s	1.3×10^{-2}	6.2×10^{-3}	1.7×10^{-3}	3.4×10^{-4}
Orbach (Fig. S33)	[a]U_{eff} (cm^{-1})	19.2	16.0	8.9	8.3
	[a]τ_0 (s)	1.67×10^{-6}	2.45×10^{-6}	6.47×10^{-6}	1.27×10^{-6}
Orbach +QTM (Fig. 6)	τ_{QTM} (s)	5.6×10^{-3}	2.5×10^{-3}	1.29×10^{-3}	3.8×10^{-4}
	[b]U_{eff} (cm^{-1})	22.8	20.1	11.4	9.4
	[b]τ_0 (s)	7.04×10^{-7}	9.01×10^{-7}	3.05×10^{-6}	1.01×10^{-6}
Raman (all *T*, Fig. S33)	[c]b ($s^{-1}.K^{-n}$)	0.35	1.59	51.62	500.81
	[c]n	5.45	4.85	3.46	2.90
Raman (below ~2.5 K)	[d]b ($s^{-1}.K^{-n}$)	19.49	37.71	127.74	671.83
	[d]n	2.28	2.53	2.60	2.52
Raman (above ~ 2.5 K)	[d]b ($s^{-1}.K^{-n}$)	1.82	6.23	51.93	221.41
	[d]n	4.45	4.00	3.44	3.37
[a] $\tau(T) = \tau_0 \exp(U_{eff}/k_BT)$; [b] $\tau(T)^{-1} = \tau_{QTM}^{-1} + \tau_0^{-1} \exp(U_{eff}/k_BT)$; [c] $\tau^{-1} = bT^n$; [d] $-\ln(\tau) = \ln b + n\ln(T)$, $b = \exp(\ln b)$					

References

(S1) B. N. Figgis and M. A. Hitchman, Ligand Field theory and its application, 2000, page 71.

(S2) M. Gerloch, Magnetism and Ligand-field Analysis, 1983, pages 525, 545 and 556.

(S3) P. D. Day, Electronic Structure and Magnetism of Inorganic Compounds, 1982, page 152.

(S4) G. L. Miessler, Inorganic Chemistry, 4th edition, 2010, page 399.

(S5) Y. Terasakia and S. Kaizaki, *J. Chem. Soc. Dalton Trans*., 1995, 2837-2841

(S6) K. Kurzak, B. Kurzak, A. Kamecka and A. Wózna, *Journal of Solution Chemistry*, 2001, **30**, 1051–1064.

(S7) N. F. Chilton, R. P. Anderson, L. D. Turner, A. Soncini and K. S. Murray, *J. Comput. Chem*., 2013, 34, 1164-1175.

(S8) M. P. Shores, J. J. Sokol and J. R. Long, *J. Am. Chem. Soc*., 2002, **124**, 2279.

(S9) R. Boča, Theoretical Foundations of Molecular magnetism, Elsevier, 1999, pages 424-425.